CHALMERS

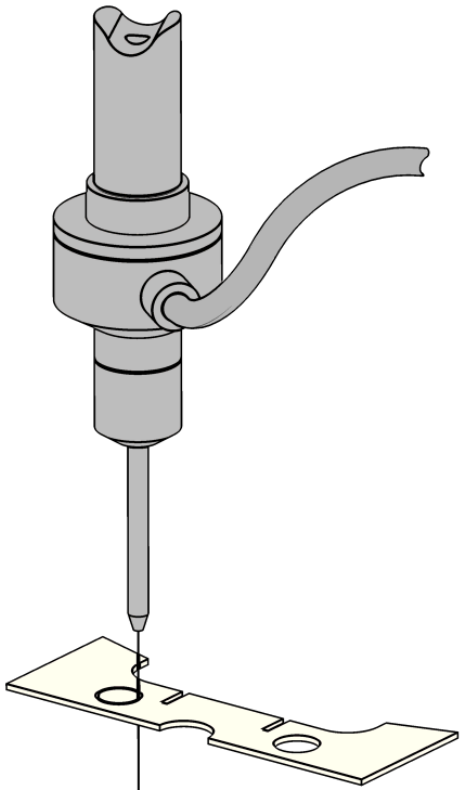

Design of Experiment and Evaluation of Abrasive Waterjet Cutting in Titanium Alloy Sheet

Diploma work in the Master programme Materials Engineering

DANIEL ANDERSSON
MIKAEL INGVARSSON

Diploma work No. 2015:167
Department of Materials and Manufacturing Technology
CHALMERS UNIVERSITY OF TECHNOLOGY
Gothenburg, Sweden 2015

Design of Experiment and Evaluation of Abrasive Waterjet Cutting in Titanium Alloy Sheet

by

DANIEL ANDERSSON
MIKAEL INGVARSSON

Diploma work No. 2015:167
at Department of Materials and Manufacturing Technology
CHALMERS UNIVERSITY OF TECHNOLOGY
Gothenburg, Sweden

Diploma work in the Master programme Materials Engineering

Performed at: GKN Aerospace Sweden
Flygmotorvägen 1, 461 38 Trollhättan

Supervisor(s): Process Engineer Joakim Idetjärn
GKN Aerospace Sweden
Flygmotorvägen 1, 461 38 Trollhättan

Lecturer Gustav Holmqvist
Department of Materials and Manufacturing Technology
Chalmers University of Technology, SE - 412 96 Gothenburg

Examiner: Head of department and Professor Lars Nyborg
Department of Materials and Manufacturing Technology
Chalmers University of Technology, SE - 412 96 Gothenburg

Design of Experiment and Evaluation of Abrasive Waterjet Cutting in Titanium Alloy Sheet
DANIEL ANDERSSON
MIKAEL INGVARSSON

Diploma work no. 2015:167
Department of Materials and Manufacturing Technology
Chalmers University of Technology
SE-412 96 Gothenburg
Sweden
Telephone + 46 (0)31-772 1000

Cover:
[The abrasive waterjet head cutting the experiment component, rendering of CAD model.]

[Chalmers reproservice]
Gothenburg, Sweden 2015

Design of Experiment and Evaluation of Abrasive Waterjet Cutting in Titanium Alloy Sheet
DANIEL ANDERSSON
MIKAEL INGVARSSON
Department of Materials and Manufacturing Technology
Chalmers University of Technology

Abstract

High demands on components in the aerospace industry empower the use of advanced manufacturing processes in order to increase quality and reduce costly processing steps. This includes non-conventional machining such as Abrasive Waterjet where the components are cut through abrasive impingement by means of abrasives accelerated by pressurized water. While avoiding effects of heating in the material, the technique entails some considerable characteristics. Thus this master thesis aims to analyze the process and experimentally study the effect of selected process parameters.

Titanium alloy sheet samples of different thicknesses were cut by abrasive waterjet while varying cutting speed, water pressure, abrasive feed and grit size with both a standard technique and a finer micromachining technique. Sections of the samples were prepared by polishing followed by etching and then analyzed through visual inspection, optical and scanning electron microscopy and XEDS analysis.

The analyses of the samples indicated varying extent of known characteristics and through statistical analysis their relations to process parameters could be assessed. Main factors of the abrasive waterjet process were found to be the material thickness and cutting speed, influencing all responses to some extent. Through the design of experiments approach it was found that some responses could be correlated to models with significance, while other correlations lacked significance due to difficulties in measurements or other error sources.

Grit embedment in the kerf was confirmed which might conflict present specifications on contamination. Yet, the consequence and distribution of grit particles needs to be considered.

Keywords: Abrasive, Waterjet, Cutting, Process window

Note from Authors

This report is a revised version of the report to GKN Aerospace. The report excludes some information, such as tables and appendices, to protect intellectual property of the company.

Thanks are extended to our supervisors Joakim Idetjärn and Gustav Holmqvist as well as to Fredrik Niklasson, Per Ingemansson and Jimmy Johansson for extra guidance during this thesis work. We would also like to thank Anders Jönsson and Tony Rydh for the help in conducting the experiments.

Daniel and Mikael, Gothenburg, June 2015

Contents

Nomenclature **viii**

1 Introduction **1**
1.1 Background . . . 1
1.2 Purpose . . . 1
1.3 Scope . . . 2
1.4 Problem Definition . . . 2

2 Theory **3**
2.1 Titanium . . . 3
2.2 Abrasive Waterjet . . . 4
2.2.1 Abrasives . . . 5
2.2.2 Characteristics of Abrasive Waterjet Cut Surface . . . 6
2.2.2.1 Erosive Machining . . . 6
2.2.2.2 Regions of the Kerf . . . 6
2.2.2.3 Difficulties in Machining . . . 7
2.2.2.4 Defects . . . 8
2.2.3 Process Parameters and Effects on Surface Finish . . . 9
2.3 Fine Abrasive Waterjet . . . 10

3 Method **11**
3.1 Parameter Selection and Ranges . . . 11
3.2 Design of Experiment . . . 12
3.3 Abrasive Waterjet Experiment . . . 13
3.4 Sample Preparation . . . 14
3.4.1 Sectioning and Mounting . . . 14
3.4.2 Grinding . . . 14
3.4.3 Polishing and Etching . . . 16
3.5 Evaluation . . . 16
3.5.1 Visual Inspection and Microscopy . . . 17
3.5.2 Scanning Electron Microscopy . . . 19
3.6 Verification of Abrasive Feed Rate . . . 21
3.7 Hardness Control of Sheet Material . . . 21
3.8 Nominal and Measured Material Thickness . . . 22
3.9 Software Modeling . . . 22

4 Results **25**
4.1 Response Modeling . . . 25
4.1.1 Taper . . . 25
4.1.2 Edge Rounding . . . 26
4.1.3 Burr . . . 29
4.1.4 Striations and Rough Cutting Region . . . 31
4.1.5 Surface Roughness . . . 34
4.2 Residual Particles Observed in SEM . . . 35
4.2.1 Composition Mapping . . . 35
4.2.2 Point Analysis . . . 35
4.2.3 Specific Particle Identification . . . 35

5 Discussion **39**
5.1 Material Thickness . . . 39
5.2 Abrasive Feed Rate . . . 40
5.3 Water Pressure . . . 40
5.4 Traverse Rate . . . 40
5.5 Abrasive Grit Size . . . 40
5.6 Abrasive Grit Type . . . 41
5.7 Grit Embedment . . . 41
5.8 Note on burr . . . 42
5.9 Extra Tests . . . 42
5.10 Uncertainties and Error Sources . . . 43
5.10.1 Experimental Setup . . . 43
5.10.2 Preparation of Samples . . . 43
5.10.3 Geometrical measurements . . . 44
5.10.4 Chemical Analysis . . . 45
5.10.5 Wear on Test Equipment . . . 46
5.10.6 Comments Regarding Statistical Analysis . . . 46

6 Conclusions **47**
6.1 Main Factors of AWJ and FAWJ Processes . . . 47
6.2 Suggestions for Further Studies . . . 47

Bibliography **49**

Appendix A Test Plan **I**

Appendix B Test Equipment **V**
B.1 AWJ Setup . . . V
B.2 FAWJ Setup . . . V

Appendix C Abrasive specifications **VII**

Appendix D Response Sheets **IX**

Appendix E Model Statistics Overview for Standard AWJ Samples **XIII**

Appendix F Model Statistics Overview for FAWJ Samples **XIX**

Appendix G Chemical Composition Mappings **XXV**

Appendix H Composition Mapping References **XXIX**

Appendix I Chemical Composition Point Scans **XXXIII**

Appendix J Abrasive Feed Calibration **XLI**

Nomenclature

t, a	Material thickness
$\dot{m}_a$	Abrasive feed rate
P_w	Water pressure
v_f	Traverse rate
s	Standoff distance
d_n	Orifice diameter
d_f	Focus tube diameter
l_f	Focus tube length
n	Striation lag
f	Striation width
h_R	Rough cutting region height
u	Taper offset
w_r	Edge rounding width
h_r	Edge rounding height
d_r	Edge rounding diameter
w_b	Burr width (root thickness)
l_b	Burr length
β	Taper angle
r_s	Surface roughness

Additional index r was used for annotation of measurements in radii.

1

Introduction

This thesis concerns the implementation of Abrasive Waterjet machining in the aerospace industry. In this sector the high demand on mechanical performance often requires deliberate and tedious thus costly manufacturing processes and alternative techniques may enable higher quality and reduce post processing. The benefits, like the limited heat impact, of the relatively young, non-conventional Abrasive Waterjet technique makes it an appealing choice. Still, the utilization of the technique lacks enough investigation according to the strict specifications controlling procedures in the aerospace industry. The experiments and evaluation this thesis aims to initiate the application of Abrasive Waterjet by studying the properties of the process and evaluating its potentials.

1.1 Background

Aerospace engineering is an area in which there are high demands on the production process, such as the forming and finishing of parts. A wide variety of production methods are used, both conventional and non-conventional. One relatively young technique which application might be useful is abrasive waterjet cutting (AWJ). Today the technique is used to some extent but require post-processing, like milling, to fulfill specifications on aerospace components. Benefits of abrasive waterjet include no heat affected zone and the possibility of cutting most materials, including hard-to-machine materials used in aerospace applications. However, research is needed regarding the effects of the process parameters, on the resulting cut components quality. Preferably, components would be cut into a clean, fine enough surfaces so that no more finishing steps such as milling are needed.

1.2 Purpose

The purpose of the thesis work is to assess the abrasive waterjet (AWJ) and fine abrasive waterjet (FAWJ) cutting methods in the manufacturing of aerospace components made from titanium alloy sheets in order to find what parameters of the process are most influential on surface finish and particle embedment. This knowledge can then be used in the establishment of requirements for using these cutting methods.

1.3 Scope

This thesis is focused on the establishment of a process window for abrasive waterjet cutting for aerospace components in sheet titanium alloy, specifically Ti-6Al-4V produced according to specification AMS 4911.

The project work includes an experimental phase where components will be cut from titanium sheets. The experiments are conducted according to a test plan utilizing factorial experiment design for altering process parameters. This enables evaluation of how parameters affect the components surface properties in the AWJ process while reducing the total amount of tests needed. Parameters are selected after consulting previous work in the area as well as through deliberation with Anders Jönsson at Swedish Waterjet Lab.

The cut surfaces of the components are evaluated through response parameters which are selected appropriately to specifications from GKN. Evaluation is intended to result in a description of cutting qualities of abrasive waterjet depending on variable parameters and a process window within the specification of aerospace components. Recommendations on continued work, such as parameters for further studies, is to be proposed.

In addition to this written report the thesis work will be presented at both GKN in Trollhättan and Chalmers University in Gothenburg.

1.4 Problem Definition

The thesis work was formulated through the following questions:

- What are the properties of the kerf from abrasive waterjet cutting and how are they assessed?
- Which are the main factors in the AWJ process?
- How does the process parameters selected influence the response parameters and the quality of the cut?
- What are the limiting aspects of the method for use in aerospace industry?

2

Theory

This chapter includes some of the theoretical background required for this thesis work.

2.1 Titanium

Titanium alloys are primarily used for their unique properties such as high strength and low density with high-temperature strength in applications where high material cost can be justified. One such application is the aerospace industry with demands on low weight components to reduce fuel consumption and high service temperatures around and inside the jet engines. Downsides of titanium use include the mentioned, high price and machining difficulties due to chemical activity and low thermal conductivity (Ramulu, Y.W., Hashish, Pedersen, and Posinasetti, 2002). Titanium forms an oxide layer in oxygenous atmosphere. This passivates the surface from further oxidation and provides resistance to chemical attack (Caron and Staley, 1997).

Ti-6Al-4V is the most commonly employed titanium alloy. Alloying with aluminum promotes alpha phase while vanadium stabilizes the beta phase. After solution treatment at above beta transition temperature the product is metastable at room temperature, which enables precipitation of alpha phase on cooling. Depending on cooling rate the alpha phase can form in different morphologies like coarse or fine acicular or needle-like grains (Caron and Staley, 1997). The precipitation hardens the alloy and increases yield strength by forming obstacles for dislocation movement.

The samples used in the experimental part are sheets of different thicknesses of Ti-6Al-4V according AMS 4911, see Table 2.1 for chemical composition. Heat treatment according to this standard involves annealing within the temperature range of 704 - 899°C for around 20 minutes followed by reheating to 718°C for 20 minutes and then air cooling or slower. This heat treatment sequence produces an isotropic alpha-beta microstructure where some variances are acceptable. Hence the microstructure of the sheets might include equiaxed, lamellar and elongated alpha grains and some discontinuous grain boundaries in transformed beta-phase matrix.

Table 2.1: Alloying composition (wt%) of Ti-6Al-4V according to AMS 4911

Ti	Al	V	Fe	O	C	N	H	Y	Other
—	5.5 - 6.75	3.5 - 4.5	< 0.3	< 0.2	< 0.08	< 0.05	< 0.015	< 0.005	< 0.4

2.2 Abrasive Waterjet

Abrasive waterjet is a manufacturing process using a high-pressure water stream entraining hard particles which on impact remove material from the subject, for example in cutting operations. The method is primarily beneficial when processing hard materials and composites and it minimizes heat impact, which otherwise might deteriorate mechanical properties in the work piece. A schematic model of an abrasive waterjet system is shown in Figure 2.1.

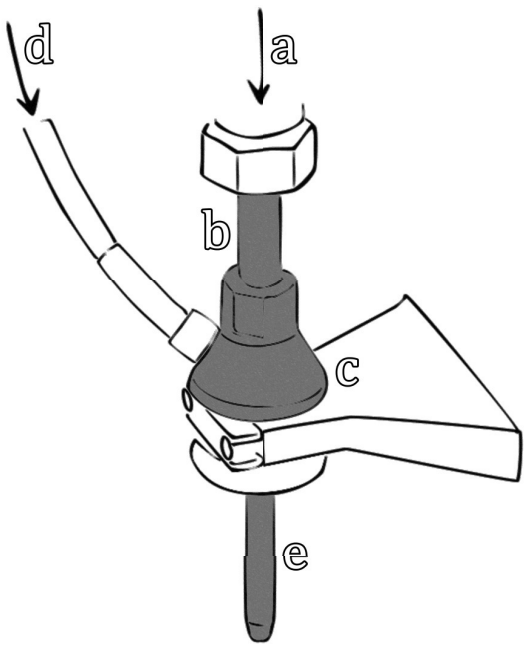

Figure 2.1: Schematic abrasive waterjet system with its main components, a) pressurized water from pump, b) pressure tube with jet forming orifice, c) mixing chamber, d) abrasive feed and e) focusing tube

The pump with intensifier generates high pressure water in the tube above the orifice, where the stream is forced through a much thinner opening. At the orifice the jet is formed as the built-up pressure is translated into kinetic energy. To withstand the eroding force of the water the orifice is produced from a hard material, typically synthetic sapphire, drastically improving its lifetime.

The abrasive particles are fed from a reservoir into the mixing chamber via an air flow from underpressure in the mixing chamber. There they coincide with the waterjet and are accelerated through the focusing tube. In some systems remaining

abrasive is flushed out by the flowing air to prevent build-up in the mixing chamber which would otherwise lead to clogging and blockage of the jet. The focusing tube is not in contact with the jet but blocks scattered water droplets and stray particles, hence reducing the subjected area of the work piece. The jet is coherent for only a certain distance from exiting the focusing tube but is diverging and forming droplets in the lower pressure surrounding below the orifice (Öjmertz, 1994).

As the abrasive laden jet impinge the surface of the work piece the hard particles constitute the primary material removal through erosion (Öjmertz, 1994). The jet thereafter removes residual particles and abraded material clearing new surface.

Accelerated particles need to be decelerated below the cut. The collector, constituted by a water filled tank just below the work piece, slows down the jet and leaves the abrasive particles at the bottom of the tank. The top of the collector is then closed off by a covering sheet. Thus the amounts of particles are minimized in the atmosphere surrounding the process.

The processed sheet is often mounted on a steel support grid. Although the process exerts minimal lateral force on the work piece, additional fixation is usually applied. The mount also prevents flexing of the material which may otherwise negatively influence the cut accuracy.

The AWJ process shapes products by moving the jet nozzle across the work piece. The motion is often executed by mounting on a x-y table, allowing for precise operations, but robots can be used for three dimensional shaping of more complex components.

2.2.1 Abrasives

Abrasive waterjet utilizes the addition of abrasive particles to enable cutting much harder materials than the pure waterjet process. Some of the main abrasive used today are olivine sand and garnet, as well as oxides and carbides like aluminum oxide and silicon carbide. Garnet is the most commonly used abrasive and it has high hardness without excessive tool wear (Mort, 1995). Garnet has a higher hardness and more even temperature stability than olivine sand (Shaw, 1996). According to Öjmertz (1994) can olivine be used in applications where the reduced abrasive cost outweigh the required decrease in cutting speed due to softness.

Garnet is a name for a group of silicate minerals of cubic crystalline form described by the formula $3AO\ B_2O_3\ 3SiO_4$ where A may be Ca, Mg, Fe^{2+} or Mn and B may be Al, Fe^{3+} or Cr^{3+} (Allaby, 2008). Some types of garnets and their properties are listed in Table 2.2. Abrasives can be reused, were particles are added back together with unused particles. Particles are broken down when cutting a surface, so recycling generally widens the distribution of particle sizes in a certain mesh, reducing its quality.

Table 2.2: Garnets and their properties (Kogel, Trivedi, Barker, and Krukowski, 2006)

Garnet	Chemical formula	Color	spec. gravity	Mohs hardness
Almandine	$3FeO\ Al_2O_3\ 3SiO_2$	Deep red, brownish red to black	4.1-4.3	7.0-7.5
Grossular	$3CaO\ Al_2O_3\ 3SiO_2$	White, pale green, or yellow	3.4-3.6	6.5-7.0
Pyrope	$3MgO\ Al_2O_3\ 3SiO_2$	Deep red to black	3.5-3.8	6.5-7.5
Spessartine	$3MnO\ Al_2O_3\ 3SiO_2$	Brown to red	3.8-4.3	7.0-7.5
Andradite	$3CaO\ Fe_2O_3\ 3SiO_2$	Yellowgreen, black, green	3.7-4.1	6.5-7.0
Uvarovite	$3CaO\ Cr_2O_3\ 3SiO_2$	Emerald green	3.4-3.8	6.5-7.0

Garnets can be obtained from different sources such as alluvial deposits, mines or industrially synthesized. Depending on origin, the morphology of abrasive particles might differ. Alluvial abrasives tend to be round and recycled sands lose the sharpness of the recently mined.

2.2.2 Characteristics of Abrasive Waterjet Cut Surface

In order to describe the cut surfaces or kerf of produced components, characteristics have to be considered and evaluated accordingly.

2.2.2.1 Erosive Machining

The cutting mechanism of abrasive waterjets derives from the particles accelerated in the waterjet interacting with the work piece material. As the abrasive particles are harder than the work piece, material is removed through a cyclic, stochastic eroding process. Hence the kerf created by this process shows certain characteristics.

The jet exhibit stochastic properties and instabilities as it interacts with the work piece, which accounts for waviness in the surface profile (c in Figure 2.2). This behavior can come from pressure fluctuations, variations in particle distribution or vibrations in the equipment as well as inhomogeneity in the machined material. Additionally, the cyclic movements of the jet through the material create striations in the kerf (b in Figure 2.2), corresponding to the width of the jet. At a smaller scale, the chipping of individual particles also produces surface roughness (a in Figure 2.2) (Öjmertz, 2004). The components and accumulated surface profile can be seen in Figure 2.2.

2.2.2.2 Regions of the Kerf

The cut surface can be divided into three regions, see 2.3. The initial deformation region (IDR) is where the jet piercing of the work piece starts. Bombarding the surface causes stray particles to create a rounding of the upper edges. The following area of the cut is the smooth cutting region (SCR) where the so called cutting wear dominates. During cutting wear the sharp edges of the harder particles chips away material of the work piece through shear. The material removed by each grain is small for the low angles of incidence hence the surface finish in this region is

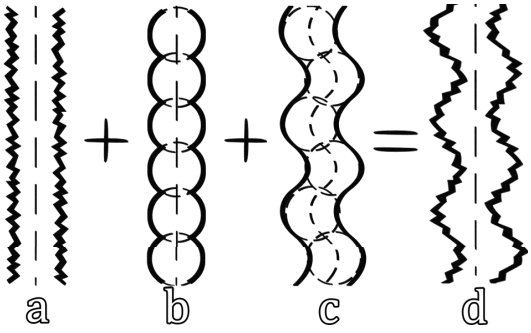

Figure 2.2: Characteristic surface profile and its components in abrasive waterjet cutting, a) roughness from individual particles, b) cyclic pattern from jet movement, c) waves derived from jet instability and d) the accumulated surface profile

fine. Further down the cut the jet trajectory curves due to the lag of the jet and creates higher angle face area. The particles collision at higher angles changes the primary mode of material removal to so called deformation wear in a striated pattern called the rough cutting region (RCR). In deformation wear the affected area erodes through cyclic impacts from the abrasive (Öjmertz, 1994).

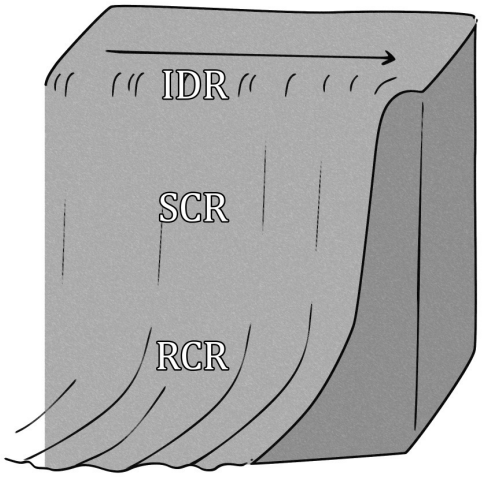

Figure 2.3: Regions of the abrasive waterjet cut kerf. IDR with piercing and impingement defects, SCR where the jet produces a rather fine surface and striated and coarse features in RCR, arrow indicates cutting direction

2.2.2.3 Difficulties in Machining

During initial penetration of the work piece, the jet is directed back up through the entrance causing irregularities. This problem is often prevented by penetration outside the final cut in discarded material or by entering the work piece from a sheet edge.

The lag of the jet results in delayed tracing of the cut deeper in the kerf which creates shape deviations, especially at higher velocities and lower abrasive feed and

pressure. This delay and inaccuracy becomes visible in corners of the cutting operation but can often by design be located in the waste material. Difficulties occur in corners inside the work piece or anywhere the lag may impact component geometry but can be counteracted by reduction of the cutting speed, through ramping. Ramping the nozzle velocity into and out of corners improves the correctness of the cut as it lets the lagging jet catch up.

The jet lag also becomes a problem when shaping holes and radii. The exit diameter then becomes larger than the face side diameter as the jet tends to stray radially due to the rotation. Tight radii bends, as mentioned corners, therefore requires lower cutting speed.

2.2.2.4 Defects

All surfaces generated by means of abrasive waterjet exhibit characteristic features from the process. One such feature is the taper of the kerf (Figure 2.4) which may pose problems to the finish of the product and requirements on subsequent processing. The taper derives from the progressing jet as it erodes material through the work piece, thus the exposure is increasing towards the face. There are ways to compensate for this defect by tilting the nozzle (Shanmugam, Wang, and Liu, 2008).

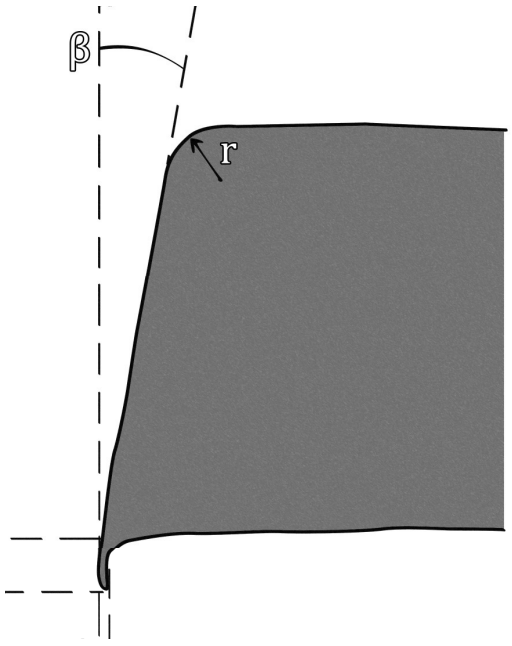

Figure 2.4: Defects in the kerf of abrasive waterjet cutting, transversal section showing taper (β), edge rounding (r) and burr of certain length and root thickness

Edge rounding (r) is the roundness around the upper kerf due to the fact that the divergence of the jet exposes more surface to erosion. The defect is indicated by the radius in Figure 2.4.

Burr forms due to the directional impingement of the jet stream plastically deforming and displacing material to the kerf exit, again see 2.4. The geometrical defect may cause problems during assembly of components, form sharp edges that are dangerous for manual handling and affect the component's performance negatively. Thus deburring is an important step in manufacturing processes. Classification is to some extent used for the evaluation of burr on kerfs, where properties such as burr length, root thickness and heat effect determines the class.

The cutting mechanism of the particles results in trails from individual abrasive grains as well as striations, see Figure 2.2, from the finite positioning of the nozzle and irregularities such as vibrations and fluctuations of the jet. Combined, these effects generate significant surface roughness compared to other cutting processes without qualified adjustments of operation parameters. As the jet particles reduce their kinetic energy their trajectory lags behind, resulting in irregular carvings. The striations constitute surface roughness that may be unacceptable and shape defects exceeding tolerances. One method of assessing the surface is through visual inspection and description with surface quality factor, Q, ranging from 1 to 5 with decreasing roughness(Zeng and Kim, 1993).

The abrasive waterjet process leaves the cut surface with embedded residual particles (Boud, Carpenter, Folkes, and Shipway, 2010). These particles might have an effect on the products mechanical performance as well as limit the joining with other parts, such as through welding.

2.2.3 Process Parameters and Effects on Surface Finish

Low water pressure in jets can be beneficial to decrease wear on equipment and increase lifetime. Higher water pressure on the other hand provides smoother surfaces and at the same time higher cutting rates. The negative effect on surface finish because of certain errors like unsteady traverse rate or uneven abrasive flow are amplified at higher pressures (Li, Wang, and Ali, 2011).

Waterjet orifice size and geometry controls the properties of jet. Larger diameters enable higher cutting depths while smaller diameters reduce depth and produce narrower kerfs (Öjmertz, 1994).

The focusing tube helps focus the jet, keeping stray particles in line and therefore reduces the exposed cutting area. A geometrically optimized focusing tube increases the energy transfer from water to abrasive particles and provides a homogeneous blend of water and abrasive. The length of the focusing tube increase momentum transfer and decrease cut width.

Abrasive mass flow rate is one of the most important parameters in abrasive waterjet cutting, controlling depth of cut and surface roughness (Shaw, 1996). A higher abrasive to water ratio increases cut depth but also kerf width. However above a

certain particle saturation, depending on the jet, maximum acceleration of the abrasives cannot be achieved and cutting performance decreases.

Abrasive grain size affects cutting depth and speed. Larger grains can carry momentum further down the cutting path, cutting deeper but with increasing unevenness. Smaller grains generally produce finer cuts as the cutting efficiency increases for each grain (Öjmertz, 1994; Shaw, 1996).

Cutting speed affects surface roughness, with a higher speed yielding a rougher cut. The kerf width increases with slower cutting speed, as the region being cut is exposed to the jet during a longer time. It is one of the most important factors in waterjet cutting quality (Li et al., 2011).

The angle of attack can change the wear mode. Tilting the jet backwards can increase the amount of cutting wear occurring, thereby yielding a smoother cut (Öjmertz, 1994).

The jet focus and pressure deteriorates after leaving the jet nozzle. Therefore, the standoff distance is important in order to cut with an effective jet. Larger standoff distance will increase the jet diameter and reduce the jets cutting efficiency. Increasing stand-off distance also results in larger IDR and more edge rounding of the cutting face. According to Shaw (1996), standoff distance is relatively unimportant as long as it is kept below one inch or 2.4 cm.

2.3 Fine Abrasive Waterjet

Developments in AWJ has led to possibilities of finer machining. It uses exactly the same principles in machining of the same materials as regular AWJ, only in smaller tool dimensions, thinner waterjet and lower abrasive flow. FAWJ machining can maximally cut about 9 mm deep, although it is mostly used in machining of less than 1 mm dimensions. To create this jet, a suspension method of abrasives in pressurized water are used instead of the standard mixing chamber (Miller, 2002).

3
Method

The project started with an initial research of abrasive waterjet manufacturing, the properties of the titanium alloy and the specific demands on the jet engine component. The research resulted in process parameters to be used in Design of Experiment (DoE) as well as properties for evaluating the quality of the product. Reduction of the number of parameters (screening) was founded on the research and consultation with Swedish Waterjet Lab in Ronneby by identifying the most significant ones and hence to decrease the number of tests needed.

The tests were performed according to the established test plans, see Appendix A, at Waterjet Lab and Waterjet Sweden in Ronneby. They included tests with two similar techniques, the standard process and a finer, more novel embodiment.The test plan was designed using the software Modde by statistically removing experimental combinations of the parameters. This enabled process parameters to be altered, the assessment of their intrinsic relations to results and the creation of the process window later. The results of varying the process was evaluated through visual inspection, microscopy of cut material and assessment of particle embedment from suitable analyses.

3.1 Parameter Selection and Ranges

The most influential process parameters were selected, see Table 3.1, during deliberation with Anders Jönsson at Swedish Waterjet Lab and according to literature Ramulu et al. (2002). These included jet pressure, standoff distance, traverse speed, abrasive size and abrasive feed rate. Furthermore, all fixed parameters, such as those shown in Table 3.2, have been chosen by Anders Jönsson through his experience but also out of convenience from available equipment.

Table 3.1: Process Parameters for standard and fine abrasive waterjet

	Standard			Fine		
Variable	Low	Center	High	Low	Center	High
Material thickness [mm]	1	3.2	6.35	1	3.2	6.35
Abrasive feed rate [g/min]	250	375	500	15	20	25
Water pressure [bar]	3000	3500	4000	3000	3500	4000
Traverse rate [mm/min]	100	200	300	30	45	60
Abrasive grit size [mesh]	80	100	120	150	200	230

The data from the table below have been excluded from this version of the report, due to the secrecy of company property.

Table 3.2: Fixed process parameters for standard and fine abrasive waterjet

Parameter	Standard	Fine
Standoff distance [mm]	-	-
Orifice diameter [mm]	-	-
Focus tube diameter [mm]	-	-
Focus tube length [mm]	-	-
Number of passes	-	
Angle of attack [°]	-	
Abrasive material	-	
Ramping	-	

Three different plate thicknesses were selected to be evaluated.

Determination of the highest cutting speed to be used in both tests was done by manual speed override until through-cutting was not achieved in the thickest samples. Lowest cutting speed was chosen as both having a high enough predicted Q-value (visual quality measurement) and because of practical reasons.

Standoff distance was fixed at an adequately small separation in this test. The influence of this parameter was thus excluded from experiments to enable the selection of the other five and could be assessed in further studies. According to Ramulu et al. (2002) standoff is one of the most influential parameters on jet penetration and kerf geometry.

Garnets were selected as abrasive for all test. The choice was based on the fact that abrasive waterjets most frequently use garnets and that they are relatively inexpensive. The mid-range hardness of garnets is also a good trade-off between cutting speed and tool wear. The details regarding the garnet used can be seen in Appendix C. Specifications as size distribution diagrams were not available. Certain garnet meshes were recycled, where up to 40 % of particles were reused.

Ramping of cutting speed to improve edge quality and geometry by reducing jet lag, was set to start 3 mm from edges of cut samples.

3.2 Design of Experiment

Fractional factorial experiment design was implemented by means of the software Modde in order to decrease the number of tests needed. Each parameter was varied between three different, justified values in the range permitted by the equipment used.

Modde then generated test plans with a randomized run orders in which to perform

the experiments to reduce effects from operator, environment and other possible sources of error.

3.3 Abrasive Waterjet Experiment

The AWJ tests and additional cutting of quality samples were done at Swedish Waterjet Lab, and FAWJ testing in Waterjet Sweden. The test setup for the two tests can be seen in Appendix B.

The cut part is an aerospace component, with design altered in order to show different effects from AWJ cutting. The same design was also used in other similar tests to facilitate comparison of experiments.

Due to difficulties in resetting machines and shortage of time some alterations of the initial test plans were necessary. In the plan for the AWJ experiments, tests with the same abrasive grit size was bunched together in pairs or triplets to lower change rate of garnet. Deviations from the random original plan were relatively small and the execution kept samples featuring the intermediate parameters evenly distributed throughout the run. Greater changes were required for the FAWJ tests where swapping of sheets was more problematic. Hence experiments on each sheet was grouped as well as the ordering of grit sizes. The complete plans for the tests can be found in Appendix A.

Samples were cut from the sheets and plate according to the revised plan while tying the position to each experiment as shown in Figure 3.1

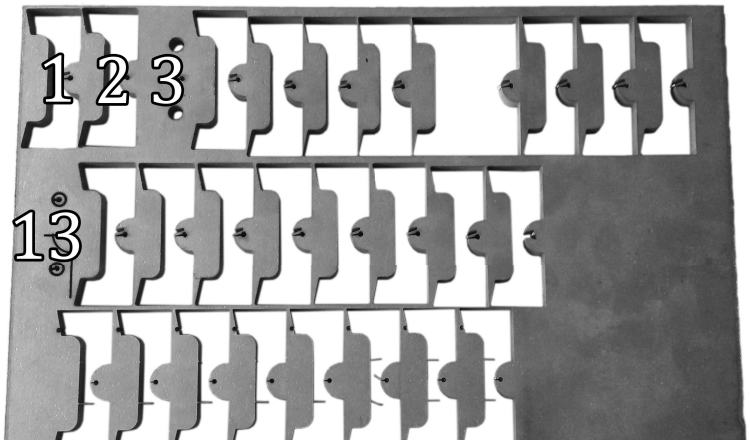

Figure 3.1: Position numbering in the sheet (see Tables A.1, A.2 and A.3 in Appendix A)

3.4 Sample Preparation

Samples cut using the two abrasive waterjet techniques were cut into sections forming transverse and longitudinal pieces of the kerf and one piece was left unprepared for analysis and preserved for future testing. Transverse and longitudinal sections were mounted in bakelite and polished for geometrical evaluations and then etched to reveal microstructure.

3.4.1 Sectioning and Mounting

Samples were separated into five sections for inspection: three pieces in the transverse direction for geometry analysis (a, b and c), one longitudinal part for surface roughness inspection (d) and one to remain as is without any sample preparation, to measure striations (e). See Figure 3.2 for reference. Arrows indicate direction for subsequent molding into bakelite.

Figure 3.2: Test samples with sections cut but not separated and named according to figure, arrows indicate the side of transverse pieces facing up in mountings

White holders where used to keep thin samples standing before molding, which can be seen in Figure 3.3. Faces of all sections were aligned towards the same direction which was then marked by the blue molding compound (grey in Figure 3.3).

3.4.2 Grinding

For grinding and polishing operations a Phoenix 4000 machine was used. The equipment features replaceable and changeable grinding papers as well as cloth for colloidal suspension polishing. Additionally the sample holder allowed for running six specimens simultaneously and applying force individually. In grinding the machine was configured to apply a force of 27 N on each sample occupied in the holder while rotating clockwise with a speed of 300 rpm. During operation water was applied continuously to the grinding plate to carry off abrasives and removed material. All samples were washed and cleaned in ultrasonic bath with soap between each abrasive grain size as well as equipment was wet and dried off with pressurized air.

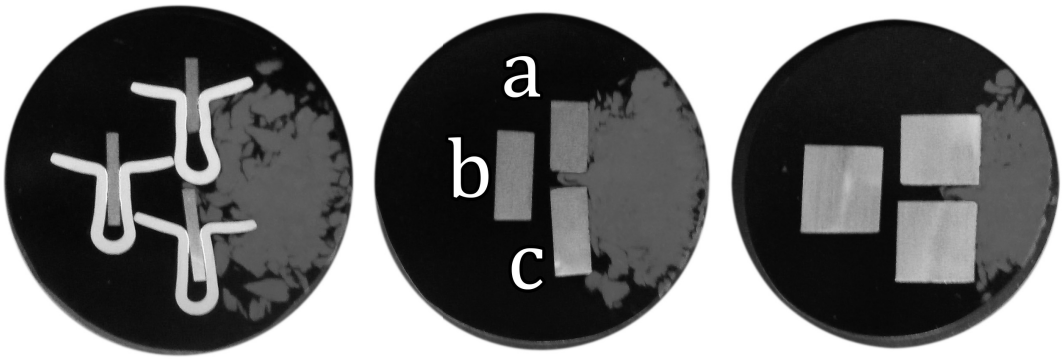

Figure 3.3: Mounted sections, sheet faces aligned towards blue molding compound (grey in image) in the order shown, white clamps were used to hold 1 mm samples upright

Grinding of transverse samples was conducted in sequence of successively finer grit size abrasive papers. Since the depth achieved in this operation was not considered affecting subsequent analysis, samples were roughly ground with 120 mesh until all sections had planar surfaces without defects from the earlier separation. Then following abrasive papers were 240, 600, 1000, 2500 and lastly 4000 mesh for 30 seconds each resulted in an adequate surface for continuing to the polishing step, according to Table 3.3.

Table 3.3: Grinding sequence for transverse samples

Grinding mesh	Duration [s]
120	30
240	30
600	30
1000	30
2500	30
4000	30

Longitudinal samples had to undergo a more precise grinding operation to ensure that the measurement depth for following surface roughness analysis was as similar as possible. Difficulties encountered concerned the defects produced in rolling of sheets in manufacturing which varied between different material thicknesses. To deal with this, separate grinding operations for each thickness had to be established. Through testing, the least amount of material removal sufficient to avoid surface defects resulted in the plan of grinding each sample to 90 % of its thickness. Through this method comparable depths were achieved.

Grinding of the thickest samples started with 40 seconds using 120 mesh abrasive paper, followed by two times with 240 mesh for 40 seconds, another 40 seconds with 600 mesh, 30 seconds with 1000 mesh, 30 seconds with 2500 mesh and finally 30 seconds with 4000 mesh (see Table 3.4).

Table 3.4: Grinding sequence for 6.35 mm longitudinal samples

Grinding mesh	Duration [s]
120	40
240	40
600	40
1000	30
2500	30
4000	30

Samples from the 3.2 mm sheet started with grinding using 240 mesh for 40 seconds before following previous sample sequence (Table 3.4) with the 600 mesh abrasive and onwards.

The thinnest samples were ground two times with 600 mesh for 40 seconds then following the operations for prior samples (Table 3.4).

3.4.3 Polishing and Etching

After grinding all samples were cleaned in an ultrasonic bath before polishing to remove any residual abrasive particles which might otherwise scratch the surface. The polishing was running for three minutes with alumina OP-S (Oxide Polishing Suspension) with grit size of 0.3 µm until mirror finish was achieved. Rotation of the sample holder was now set to counterclockwise for efficient removal of grinding scores while rotational speed was lowered to 150 rpm and with actuating force still at 27 N each.

Polished samples were inspected using optical microscope prior etching to reveal any potential flaws and defects, such as cracks. Examination before exposing microstructure is important to understand variations posed by e.g. sample preparation.

According to instructions from the sample preparation guide the etching agent Krolls (92 vol.% H20, 6 vol.% HNO3 and 2 vol.% HF) was selected. After testing different exposure times, the duration of 30 seconds was selected as this resulted in visible microstructure with proper contrast. Etching was terminated with water and cleaned in ultrasonic bath with soap before rinsed with ethanol and dried with fan. Protective caps were put on each sample to prevent contamination and damage of the surfaces during storage.

3.5 Evaluation

By studying the geometrical characteristics and defects created in the cutting process of the sections, evaluations of the result of each sample could be made. Transverse

sections were used to assess kerf geometries as edge rounding, taper and burr while the surface roughness could be measured on longitudinal sections. Striations and embedment of abrasive particles were studied through the unprepared pieces.

3.5.1 Visual Inspection and Microscopy

Kerf taper was analyzed on prepared, transverse sections in stereo microscope at 10x magnification, see Figure 3.4. While aligning horizontal lines with the face and the lower side of the sheet, the offset created by the taper was measured by approximation with two vertical rulers. At the same time rough estimation of the edge roundness was obtained by placing circles (d_r) at the kerf entrance.

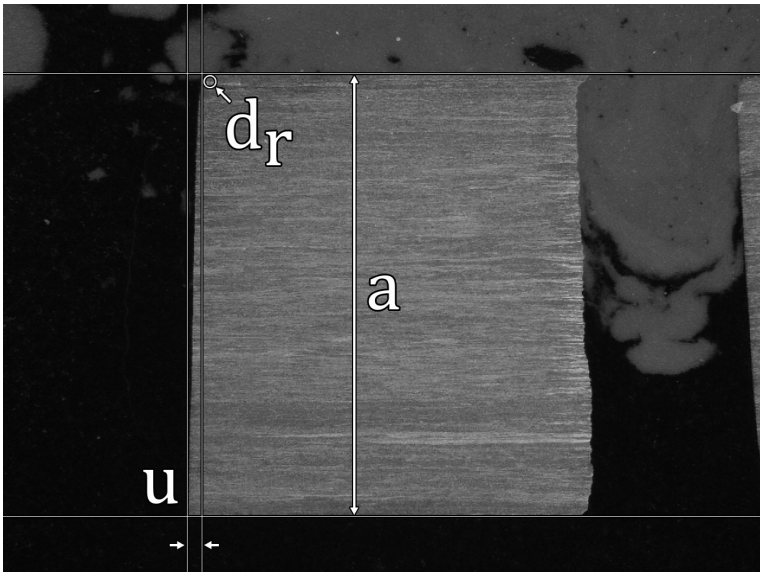

Figure 3.4: Method of taper measurement, horizontal rulers for aligning the section and measuring thickness (a) and vertical lines for the offset (u) between kerf entrance and exit, measurement of edge rounding (d_r) by fitting a circle to the curve

The initial measurements of edge rounding were done through estimation by fitting a circle diameter (d_r). This measurement was supposed to be too imprecise and it was then complemented with another measurement, width (w_r) and height (h_r) of the roundness, see figure 3.5 below.

Burr length and root thickness were measured on the transverse samples at 200x magnification using light optical microscope. These two measurements are commonly used in burr classification. Some of the samples had arched burr, but this was measured with the straight ruler along its longest side, see Figure 3.6 below.

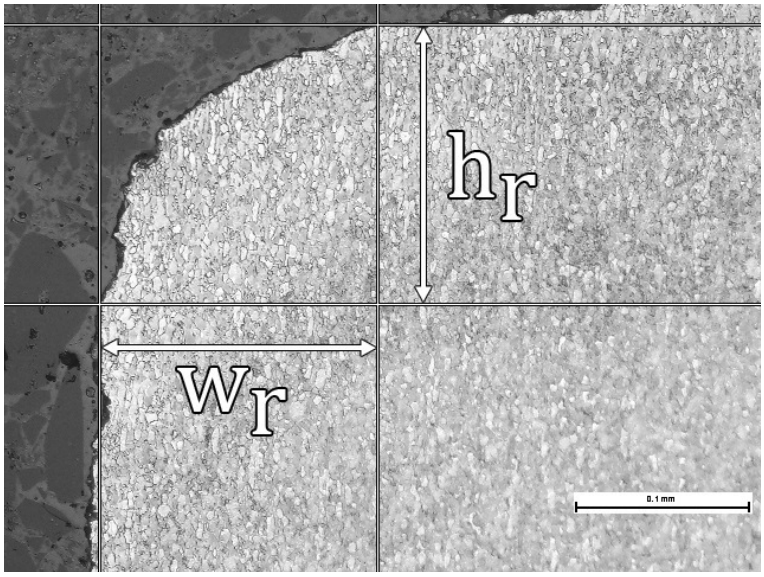

Figure 3.5: Evaluation of edge rounding by measuring height (h_r) and width (w_r) of the chamfered kerf entrance

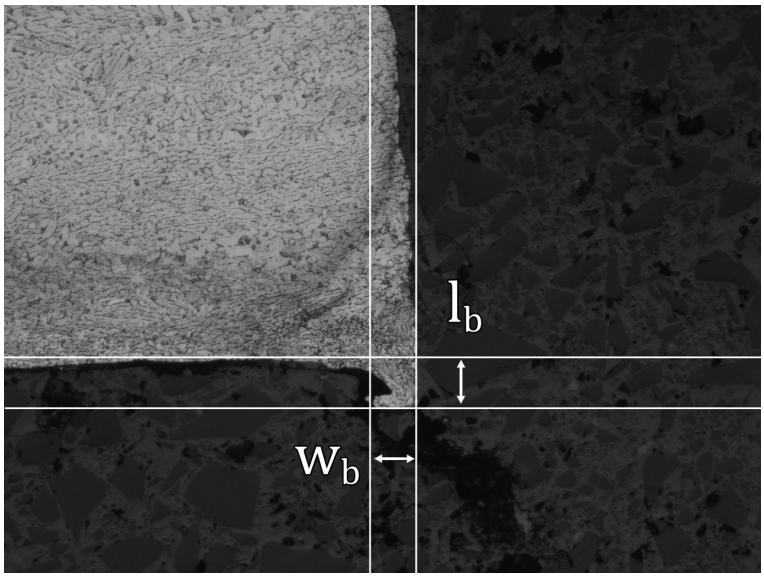

Figure 3.6: Burr on transverse section quantified through length (l_b) and root thickness (w_b) which are commonly used in classification

Striations were quantified through visual inspection using stereo microscope while enhancing their attributes with an external, tilted light source. The unprepared sections of the sample were used (e in Figure 3.2), striation lag and width and height of the rough cutting region (f, n and h_R, respectively) were measured on three sides of each piece, seen in Figure 3.7. The measurements were conducted approximately 10 mm from the corners to avoid the 3 mm of speed ramping and jet stability variations in their proximity.

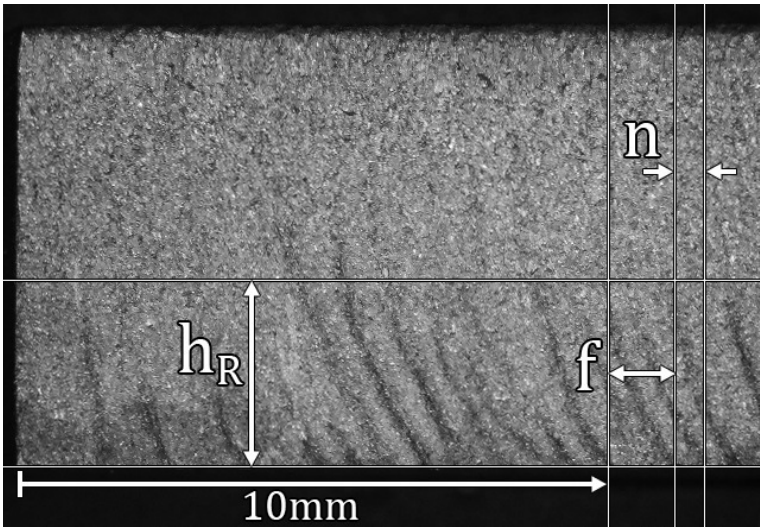

Figure 3.7: Measurements of striations in unprepared sections done in stereomicroscope, f is the trajectory deflection, n is the interval between striations and h_R is the striated area of the cut (RCR), a clearance of about 10 mm was left to avoid velocity ramping effects

Surface roughness was examined by measuring surface roughness at 16 random positions (8 on straight edges and 8 in radii) for the longitudinal sections (d in Figure 3.2). Measurements were collected in groups of four from both straight cuts and radii according to Figure 3.8 and Figure 3.9. While exploiting the full reference length range of around 800 µm in the straight areas (Figure 3.8), evaluation of round surfaces had to be narrowed down to 250 µm of the center to exclude the curve effect (Figure 3.9). Still, the roughness in radii was restricted to distinct features by the observer.

3.5.2 Scanning Electron Microscopy

The amount of residual particles was analyzed with XEDS in a SEM. The detector picks up characteristic X-rays from excited atoms in the material surface, from a volume of about 1 μm^3 from a spot of the electron beam or from a scanned area at the used acceleration voltage of 20 kV, and is decent for qualitative analysis. However, the analysis can also provide quantitative estimations as well as scanning a selected area for assessment of distribution of elements (mapping).

Certain samples were selected for analysis due to time constraints. Most samples were not cleaned, resulting in grease and organic particles left on the surface. One sample was tested both without cleaning and then after cleaning.

A group of high and low parameter values that were deemed most relevant was chosen. Tests done were: i) one mapping over a large area, ii) one picture for reference at 25x magnification and iii) to complement the mappings, three analy-

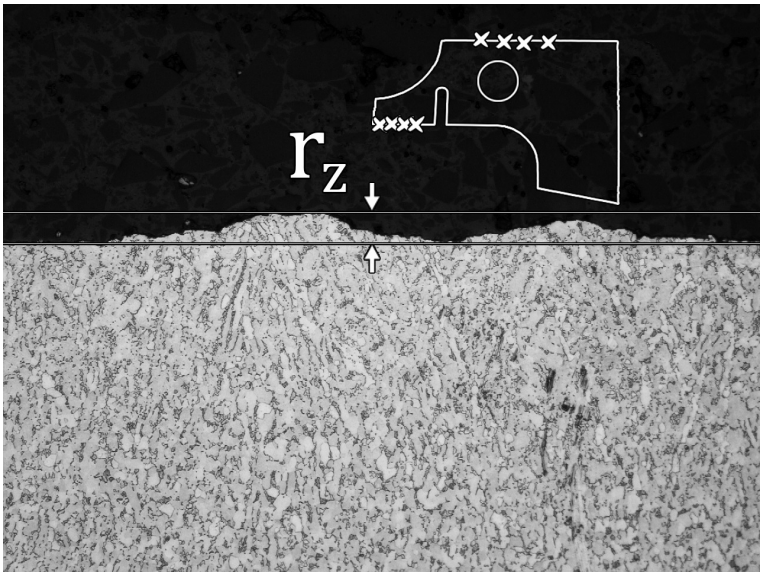

Figure 3.8: Roughness measurement (r_z) specification for straight edges over the reference length around 800 µm, crosses on the included silhouette indicate the approximate location of the random data acquirement

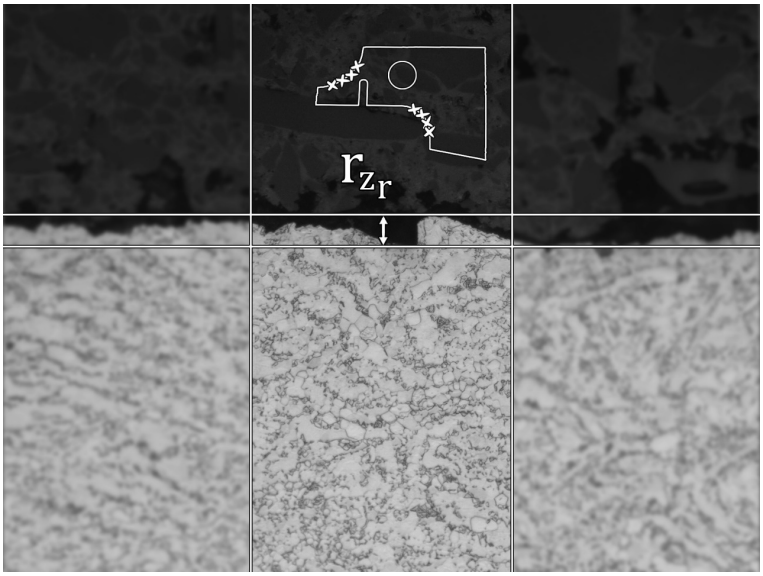

Figure 3.9: Roughness measurement specification for radii (r_{z_r}), borders restrict the reference length to around 250 µm, reducing the influence of the curve of the surface

ses of chemical composition in points, selected at 100x magnification on each sample.

The mapping was done on the top area of section e seen in Figure 3.2. The area measured was not big enough to capture the entire height of the 6.35 mm thick sample, but the 3.2 and 1 mm thick samples were covered from top to bottom. The XEDS mappings were taken in the middle of the area were no big organic particles were present. The mappings consisted of $5 \cdot 10^6$ point measurements over the area.

The scanning electron microscope was also used to capture some images and chemical compositions of encountered abrasive and organic particles.

3.6 Verification of Abrasive Feed Rate

Calibration of abrasive feed rate was done beforehand on the standard AWJ cutting machines. In the FAWJ tests, the feed rate was measured manually for two minutes and then weighing the sand. This was done for all three sand meshes used, three times for each type. As can be seen below in Figure 3.10, the 200 mesh sand deviates. The other two types are about 5 g/min under input value across all inputs. For the complete calibration measurements, refer to Appendix J.

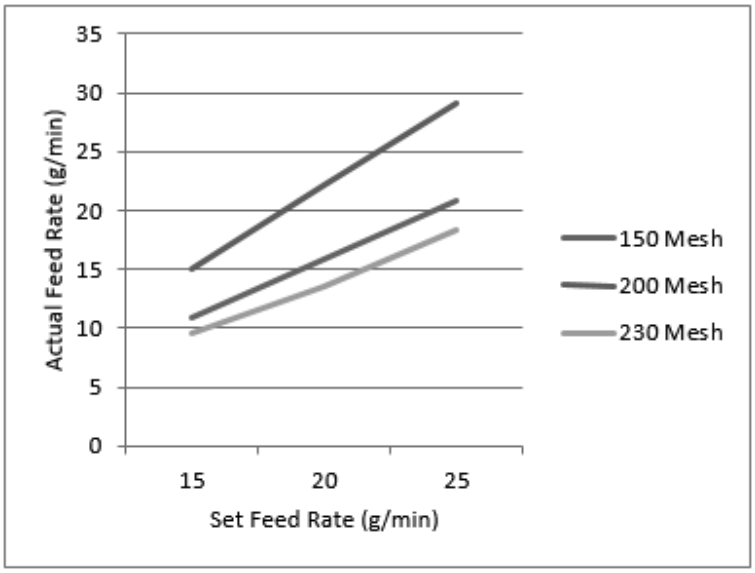

Figure 3.10: Plot of set feed rate vs. actual feed rate, reference data in Appendix J

3.7 Hardness Control of Sheet Material

The titanium base material sheets were evaluated in terms of hardness in a Vickers test, with 300 grams load. An average from three values on random points from each sheet thickness was taken, see Table 3.5. Though this was not statistically conclusive, the results were used to verify that the microstructure after heat treatment are comparable between different material thicknesses and assuring the influence on responses was minimal.

Table 3.5: Average Vickers hardness for each plate thickness

1 mm	3.2 mm	6.35 mm
324 Hv	323 Hv	331 Hv

3.8 Nominal and Measured Material Thickness

Obvious deviations of measured material thicknesses in relation to the sheets specifications led to requirements on amendments. Certain variances are permitted by tolerances and were to be expected for the material. Nevertheless, improvements to the analysis were made through replacing the nominal dimensions with the measured values. The discrepancy of the material thicknesses from nominal values is shown in Table 3.6.

Table 3.6: Correlation between Nominal thickness and measured average, data can be seen in Appendix D

Nominal thickness	Average measured thickness
1 mm	0.967 mm
3.2 mm	3.154 mm
6.35 mm	6.845 mm

3.9 Software Modeling

The statistical analysis of previous cutting experiments and evaluation were carried out in the software Modde. Hence, the terminology from the software is used (Wold, Trygg, Berglund, and Antti, 2001; Bisgaard and Kulahci, 2006). After importing parameters and measured response values for all test, the data was systematically fitted to models through PLS (Partial Least Square) regression and MLR (Multiple Linear Regression). Transformations of some factors were applied to improve models and exponential dependencies were identified in multiple models. In each experiment, the replicates (Figure 3.11a and Appendices E and F) of the response parameters were considered for an initial evaluation of measurement variations.

Four columns for each response in the Summary Fit Plot (Figure 3.11b and Appendices E and F) indicate the evaluations robustness and the conformity of the model, through model fit, cross validation, model validity and reproducibility. High columns indicate good model fit and can be improved through factor transformations or exclusion. In order to maintain some statistical rigidity minimum values of each model conformity indicator were adopted according to the guide integrated in the software and recommendations from the instructor of the analysis method.

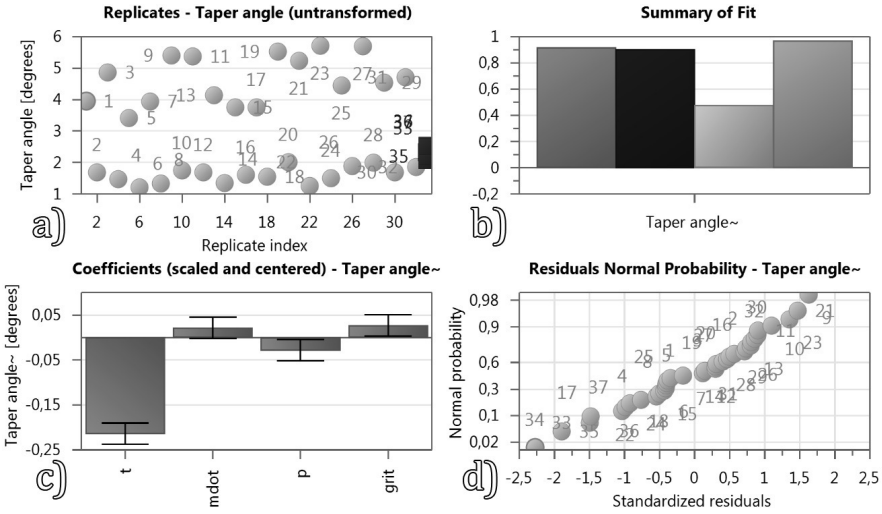

Figure 3.11: The four overview plots from Modde for taper angle, a) Replicates, b) Summary of Fit, c) Coefficients and d) Residuals

The distribution of measured values for the responses was visualized in Histogram Plots. By studying the distribution certain patterns of correlations could be assessed. A normal distribution was desirable for influences lacking dominant relations since this would indicate a proper design of experiment and method of measurement.

Model fit indicates how well the model fit the data through the variation of the response in the model. The model fitting value will be low if experimental errors are poorly controlled (low reproducibility) or the model is improper (low model validity). A minimum of 0.6 was set.

Cross validation is the ability of the model to predict new data expressed as the estimated precision of future predictions via cross validation. Values greater than 0.5 are desired to ensure significant predictions.

Model validity represents the model problems such as presence of outliers or incorrect model or factor transformation. Above model validity of 0.25, the model error is in the same range as the pure error (no lack of fit), why it was selected as target.

Reproducibility is the indicator of the accuracy of the response evaluations based on the consistency of the values from the equal, mid-range process parameters in 3.2 mm sheets. Deviations of these measurements show if the methods of assessment are problematic and resulting in questionable conclusions. The threshold for reproducibility should be high and was set to 0.8.

The confirmation of parameter significance and exclusion of non-significant parameters was contemplated through Coefficient Plots (Figure 3.11c and Appendices E and F). The impact of each parameter, regression coefficient, on the responses is here visible with whiskers indicating the confidence interval (95%). In case of notable

impact in addition to relative low noise the parameter could be considered significant. Exclusion of parameters was performed systematically through trial and error while consulting the model conformity until an optimal value for Q2 was attained.

Residuals (Figure 3.11d and Appendices E and F) that are linear indicate a normal distribution with observed patterns. This shows that there was no systematic error in the evaluation.

Contour plots are used to display the effect of two factors on one response parameter. One example is used in Figure 3.12. Response values are shown in the white boxes.

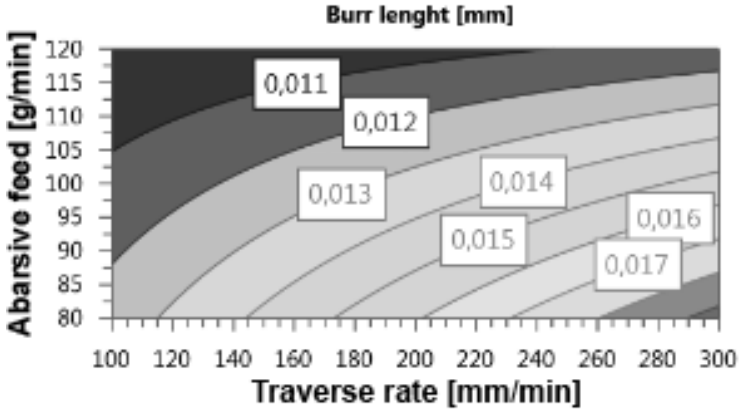

Figure 3.12: Contour plot of burr length with response values indicated by colored regions and shown in the white boxes

4
Results

Defects on the kerf geometry as described in chapter 2.2.2.4 were found and assessed. This chapter presents the result from the software modeling and observations of residual particles in the cut samples.

4.1 Response Modeling

The analysis is presented and commented in the order of the graphs from Modde, as described in chapter 3.9, and separately for each output parameter.

Defects and irregularities as well as difficulties in observing response characteristics in comparable magnification led to inconsistency in measurements, rendering some responses questionable for analysis and unfit for modeling. The magnitude of impact along with the confidence interval excluded some process variables from models through insignificance.

4.1.1 Taper

The high consistency of replicates when measuring taper width and material thickness to calculate the angle of the taper proved the evaluation viable for conclusions, see Figure 3.11a. The exponential transform of the response greatly improved the model conformity with a normal distribution of the histogram plot. The summary of fit for the model showed high values on all four columns, this suggests a rather good model fit of the process influence on taper (Figure 3.11b).

Standard AWJ samples indicated high dependence of material thickness on taper, which can be seen in Figure 3.11c. Water pressure and grit size as well as abrasive feed rate had some significance though the noise was conspicuous. The residual plot was almost ideally distributed without any outliers.

For the FAWJ samples another set of parameters emerged. Again, the sheet thickness was the most prominent along with cutting speed which indicated significant impact on the taper angle; the coefficients were proportional to the previous and inversely related to the latter, as shown in Figure F.10 in Appendix F. Some influence of abrasive feed rate and its combined effect with material thickness can also be observed.

As reference the average taper angles for the different sheet thicknesses are listed below in Table 4.1.

Table 4.1: Average taper angle for material thicknesses in both AWJ and FAWJ

Sheet material thickness	Average taper angle (Standard / Fine)
1 mm	4.6 / 1.9 °
3.2 mm	2.3 / 0.7 °
6.35 mm	1.6 / 0.7 °

Following contour plots in Figure 4.1 and 4.2 show the most important factors affecting taper.

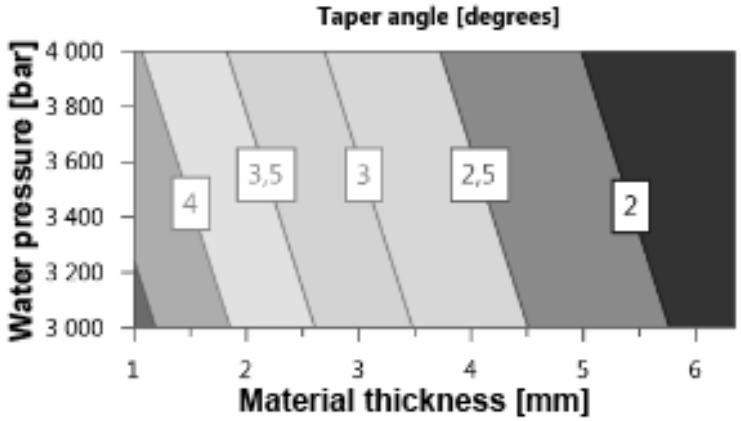

Figure 4.1: Contour plot of taper angle, against water pressure and thickness for standard AWJ

4.1.2 Edge Rounding

The measurements on edge rounding in the kerf entrance were consistent with theory (see chapter 2.2.2.4). The three measurements on edge rounding defects in the kerf entrance showed varying accuracy of measured replicas, larger range for height and width and narrow interval for the diameter method, which can be seen in Figures E.7-E.9 and F.7-F.9 in Appendices E and F, respectively. No transformations of these regression factors were made to redress the rather low Summary of Fit.

For the standard cutting tests, the diameter response showed significant influence from material thickness and the combination of thickness and pressure had some significance. Further lower impact came from thickness combined with cutting speed and abrasive feed rate combined with pressure and cutting speed and water pressure

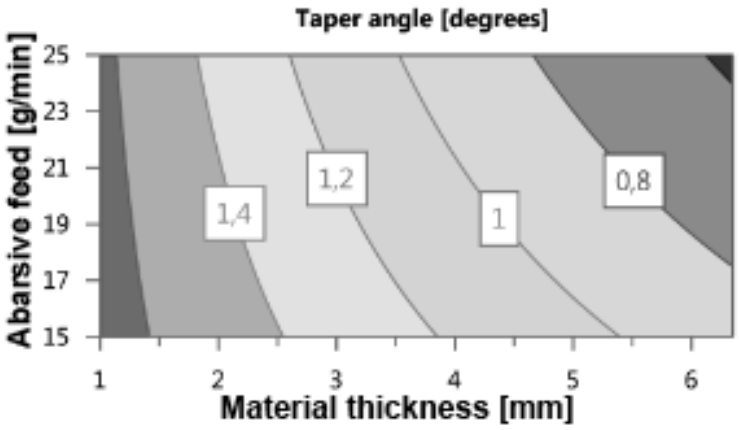

Figure 4.2: Contour plot of taper angle, against abrasive feed and thickness for FAWJ

separately. However, high confidence intervals in these, especially the separate parameters, made them non-significant but yet improving the precision of the model. All residuals were quite linear (Figure E.7 in appendix). Figure 4.3 show a contour plot for the edge rounding diameter response.

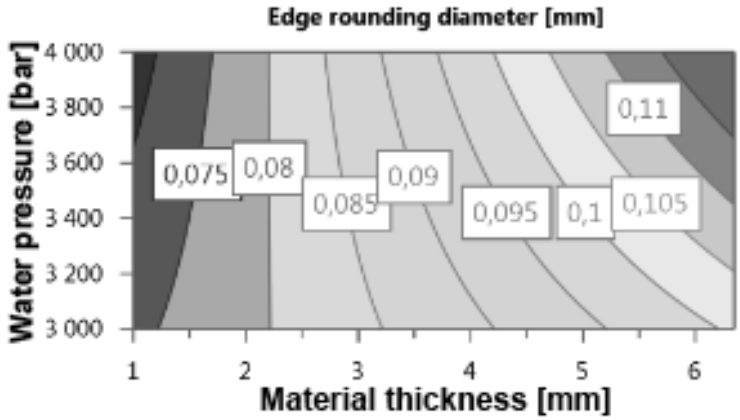

Figure 4.3: Contour plot of edge rounding diameter, against water pressure and thickness for standard AWJ

The poorest fitting model was the height of the rounding, with low reproducibility. Factors that showed significance were abrasive feed and the combination of material thickness and traverse rate. Abrasive feed rate in combination with cutting speed and thickness as well as sheet thickness and cutting speed separately also showed some influence, here listed in decreasing order of significance (Figure E.8 in appendix) and contour plot (Figure 4.4).

Edge rounding width measurements had decent reproducibility but the model lacked significance according to the Summary of Fit. Coefficient Plot indicated significance

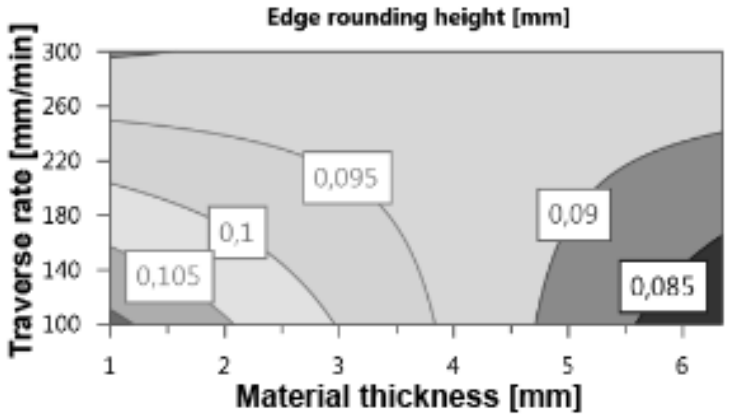

Figure 4.4: Contour plot of edge rounding height, against cutting speed and thickness for standard AWJ

of abrasive feed rate and influences from water pressure and their combination (contour plot in Figure 4.5). Again, the two most recent were rendered non-significant due to the width of the confidence interval (Figure E.7 in appendix).

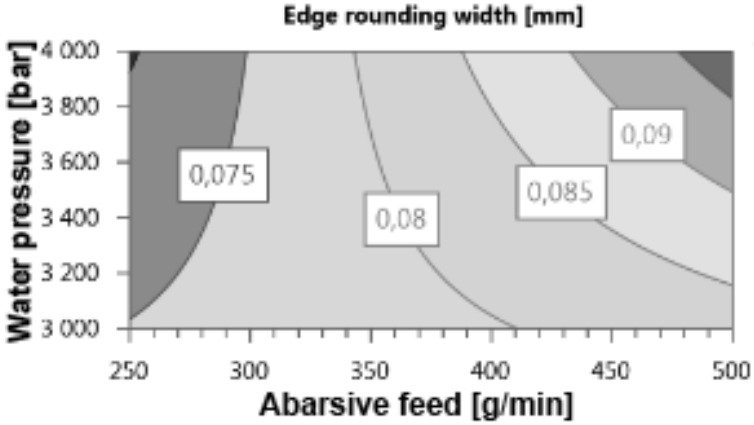

Figure 4.5: Contour plot of edge rounding width, against for water pressure and abrasive feed standard AWJ

The fine cutting in the radius had better model fit. No parameters were non-influential. The most influential parameter was thickness, followed by the four factors: i) thickness and abrasive feed (see Figure 4.6), ii) pressure and cutting speed, iii) pressure and grit size and iv) cutting speed and grit size (Figure F.7 in appendix).

The height measuring had bad replicates, yielding negative reproducibility. The overall fit was questionable, except for model validity. The most important factors were grit, thickness and abrasive feed (Figure 4.7), abrasive feed and pressure, and cutting speed and grit (Figure F.8 in appendix).

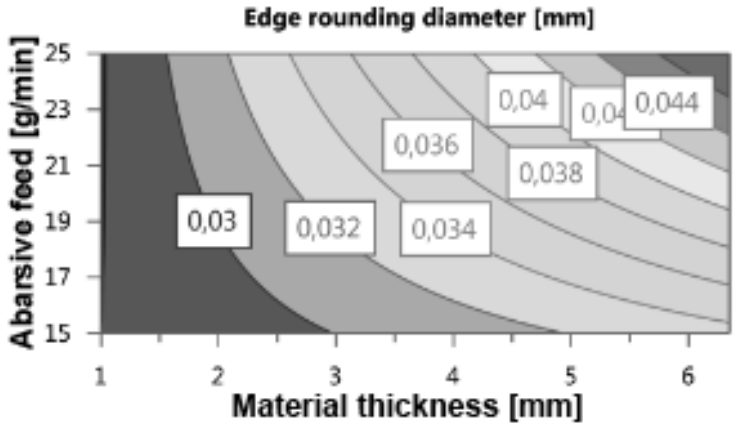

Figure 4.6: Contour plot of edge rounding diameter, against abrasive feed and thickness for FAWJ

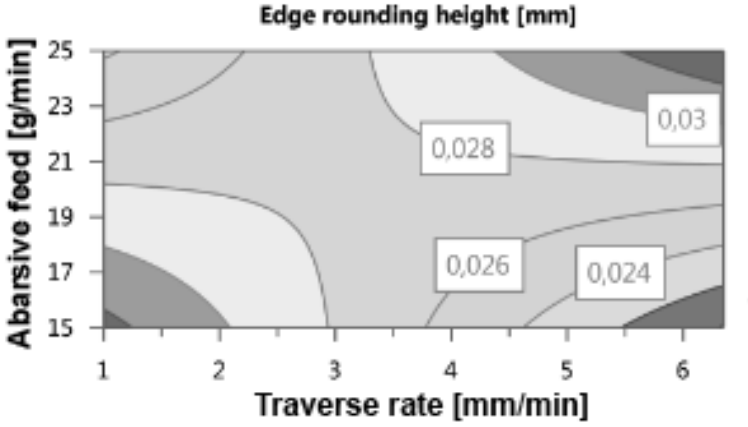

Figure 4.7: Contour plot of edge rounding height, against abrasive feed and thickness for FAWJ

Width measurements had quite low fit. The main significant factor was abrasive feed, but there was a minor effect from abrasive feed and pressure combined (Figure F.9 in appendix and Figure 4.8).

4.1.3 Burr

Burr as indicated in chapter 2.2.2.4 were found on most samples. In the standard sample measurements of burr length and root thickness, quite consistent set of replicas was observed, shown in Figures E.11 and E.12 in Appendix E. The range of the replicas corresponded to the spread of measurements on samples, thus were narrower for the burr root thickness. Still, difficulties in the model for root thickness were implied by the Summary of Fit.

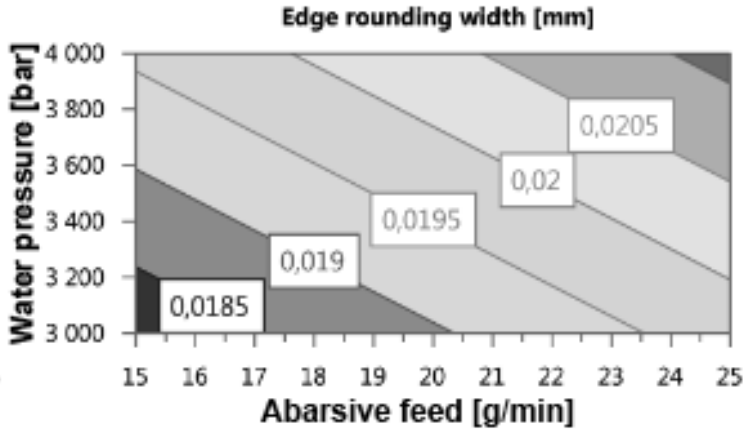

Figure 4.8: Contour plot of edge rounding width, against water pressure and abrasive feed for FAWJ

The most influential factors on the burr length were thickness and the combination with both water pressure and grit size and the latter separately. Cutting speed and grit size were less significant. The combinations of traverse rate with abrasive feed as well as with grit size turned out potentially influential, still non-significant (Figure E.11 in appendix and Figure 4.9 below).

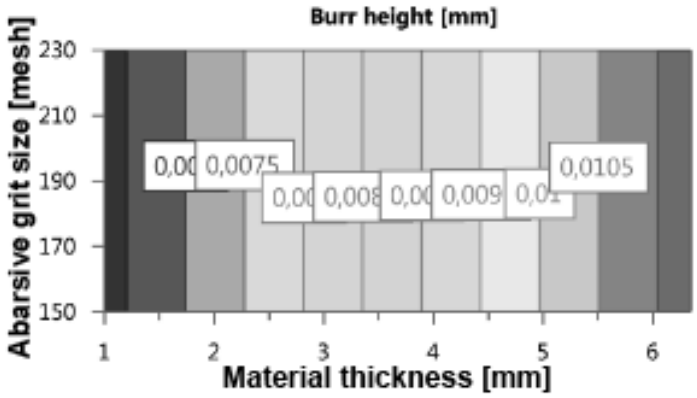

Figure 4.9: Contour plot of burr height, against abrasive grit size and thickness for standard AWJ

Regarding burr thickness, the fit was bad. Results were unreliable and therefore disregarded. (Figure E.12 in appendix).

Measurements of both burr length and root thickness on fine cutting samples were too unreliable for the results to be examined (Figures F.11 and E.12 in appendix).

The average burr size measurements are shown below in Table 4.2.

Table 4.2: Average taper angle for material thicknesses in both AWJ and FAWJ

	Standard AWJ	Fine AWJ
Average burr length	13.2 μm	8.8 μm
Average burr root thickness	9.8 μm	5.4 μm

4.1.4 Striations and Rough Cutting Region

The measurements resulted in a clearly defined lag height, for some samples, as described in Figure 2.3 in chapter 2.2.2.2, and no distinguishable line in other cases. The lag and interval between striations and the rough cutting region presented flawless replicas due to the zeros noted for samples without evaluable features. This created problems in modeling through difficulties in transformation of responses and validation due to few non-zero values. Otherwise, there was a good fit for all the above result parameters. (Figures E.1, E.3, E.5, F.1, F.3 and F.5 in appendix)

For both the standards and fine samples, shared influential factors on lag were thickness, cutting speed and the combination of the two. Abrasive feed and thickness together with abrasive feed was also important, but at varying significance for the two cases (Figures E.1 and F.1 in appendix as well as contour plots in Figures 4.10 and 4.11).

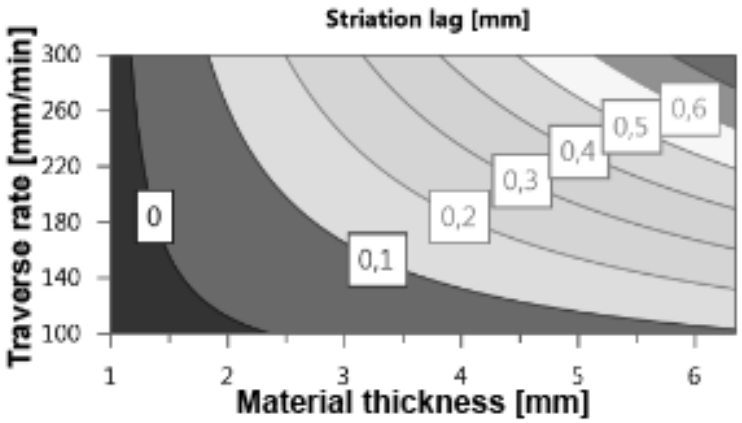

Figure 4.10: Contour plot of striation lag, against cutting speed and thickness for standard AWJ

Regarding striation width, the factors most influential in standard cutting was thickness, cutting speed and their combination, wherein the fine cutting case it was thickness and the product of cutting speed and grit size (Figures E.3 and F.3 in appendix and contour plots in Figure 4.12 and 4.13).

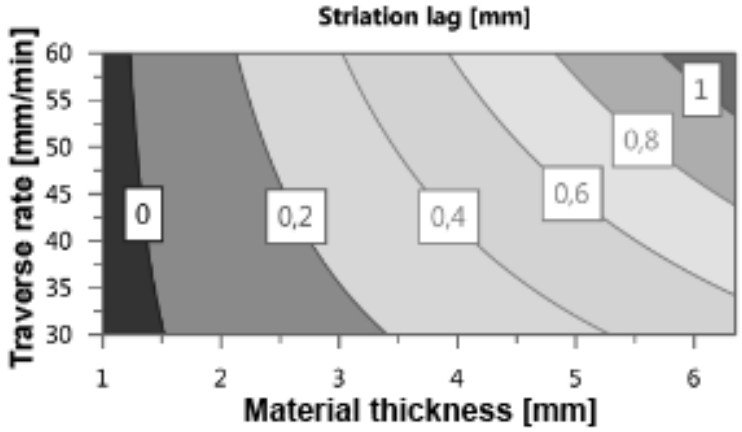

Figure 4.11: Contour plot of striation lag, against cutting speed and thickness for FAWJ

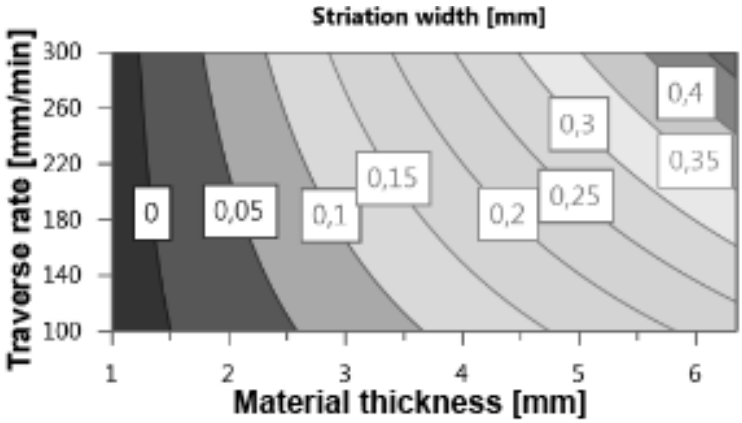

Figure 4.12: Contour plot of striation width, against cutting speed and thickness for standard AWJ

Rough cutting region was mainly affected by thickness, cutting speed and their combination, whereas thickness was the only notable factor in FAWJ (Figures E.5 and F.5 in appendix and Figures 4.14 and 4.15 below).

Residuals for all above responses showed a similar distinct non-linear behavior, an example is given in Figure 4.16 and shown individually in respective appendix.

Results from radius measurements were very similar to their straight counterparts. (See Figures E.2, E.4, E.6, F.2, F.4 and F.6 in appendix)

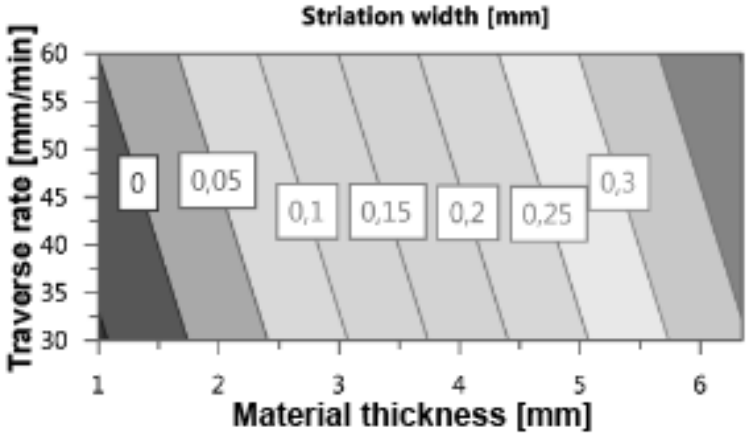

Figure 4.13: Contour plot of striation width, against cutting speed and thickness for FAWJ

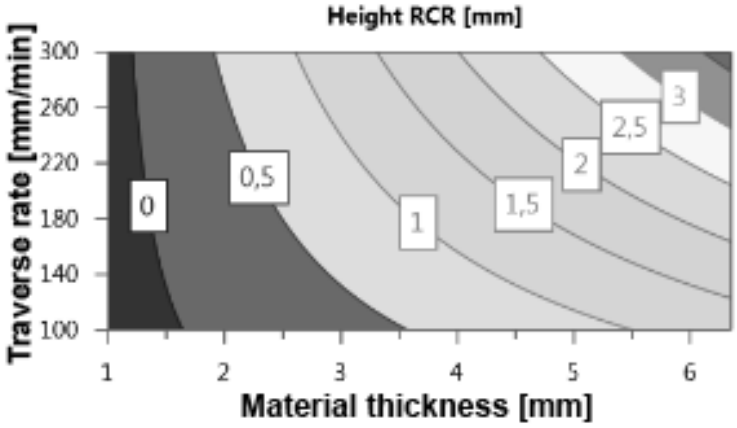

Figure 4.14: Contour plot of RCR height, against cutting speed and thickness for standard AWJ

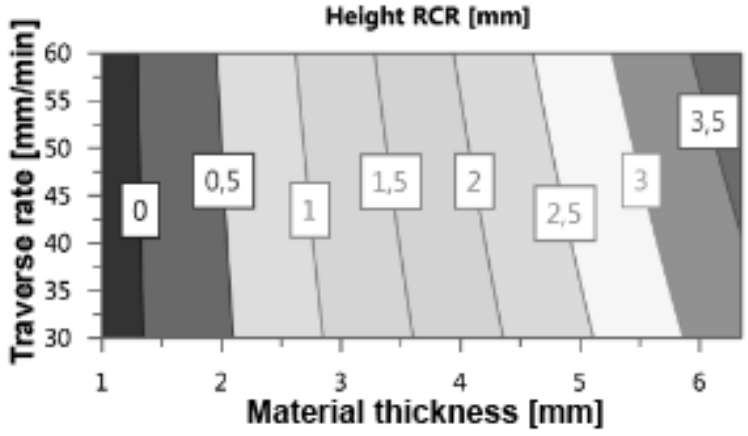

Figure 4.15: Contour plot of RCR height, against cutting speed and thickness for FAWJ

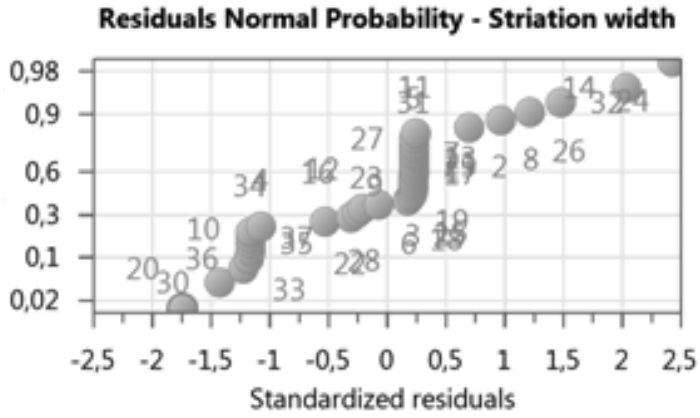

Figure 4.16: Residual plot of striation width response for standard AWJ, exemplifying non-linearity

4.1.5 Surface Roughness

The kerf exit was examined and showed the behavior described in Figure 2.2, chapter 2.2.2.1. The model fit for standard cutting on straight distances was poor except the reproducibility. The important coefficients were cutting speed and thickness, shown in contour plot below (Figure 4.17). The radius measurements deviated quite a bit, between 10-75 μm. The fit was roughly similar, with the exception of reproducibility, which was very low as well. No distinct affecting coefficient could be distinguished (Figure E.13 in appendix).

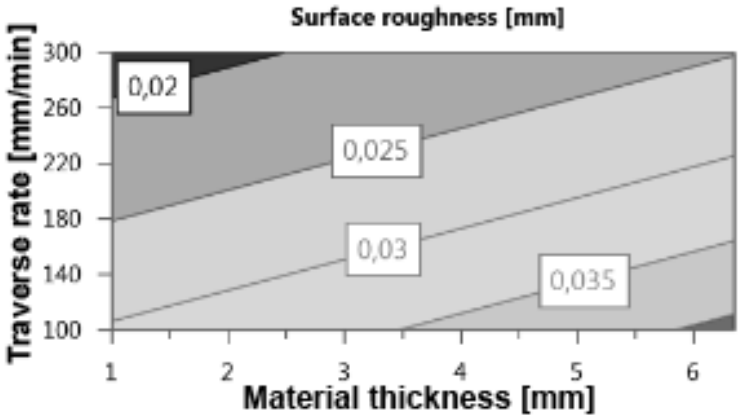

Figure 4.17: Contour plot of surface roughness, against cutting speed and thickness for standard AWJ

Fine cutting had notably high fit and was affected by thickness, abrasive feed (Figure 4.18) and their combination, cutting speed and thickness combined with cutting speed. Here, the radius version showed similar results overall for all four graphs, except only with much lower model validity (Figure F.13 in appendix).

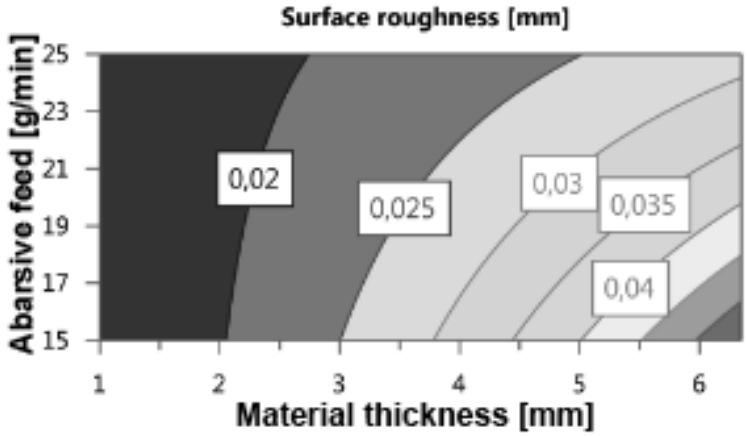

Figure 4.18: Contour plot of surface waviness, against abrasive feed and thickness for FAWJ

All residual plots for surface roughness modeling showed linear behavior.

4.2 Residual Particles Observed in SEM

The analysis for residual particles included composition mapping over an area along with three point measurements. Also, extra point analyses were done initially to identify and confirm the existence of SiO particles, as well as organic "dirt" particles.

4.2.1 Composition Mapping

Silicon content was used to monitor the presence of abrasive particles. Silicon is a constituent of any garnet type (2.2) and only minimal concentrations may occur in Ti-6Al-4V, see chapter 2.1. The wt% of Si is expected to relate to the amount of garnet on the sample surface. The results of Si content for each tested sample are shown in Table 4.3. For full results of the analyses, refer to Appendix G. For reference, a picture was taken for each analyzed area, see Appendix H.

4.2.2 Point Analysis

The results from the three point analyses on each sample are shown below in 4.4. Refer to Appendix I for full presentation of recorded spectra.

4.2.3 Specific Particle Identification

Specific point scans were performed in order to validate existence of abrasive and organic particles. Below can be seen the resulting analysis with X-ray peaks recorded from an abrasive particle and an organic particle, see Figure 4.19 and Figure 4.20, respectively. Note the high silicon content, that indicates the abrasive particle, and the high carbon content of the organic particle.

Table 4.3: Content of silicon, from XEDS anlyses, of cut sample surfaces, including measurement on a cleaned sample according to procedures described previously

Exp. number	wt% Si
S1	1.1
S2	1.2
S15	0.9
S16	1.0
S17	1.2
S18	1.1
S31	1.0
S32 (Cleaned)	1.0 (1.1)
S33	1.0
Average	1.06

Table 4.4: XEDS analyses of samples including measurement on cleaned sample

Exp. number	wt% Si, point 1	wt% Si, point 2	wt% Si, point 3
S1	1.0	1.0	0.8
S2	1.1	1.0	1.2
S15	0.8	0.8	0.8
S16	0.7	0.2	1.1
S17	1.1	1.0	1.2
S18	1.1	1.1	1.1
S31	0.9	0.8	0.9
S32 (Cleaned)	1.1 (0.8)	1.0 (1.1)	1.0 (1.1)
S33	0.9	1.2	0.8

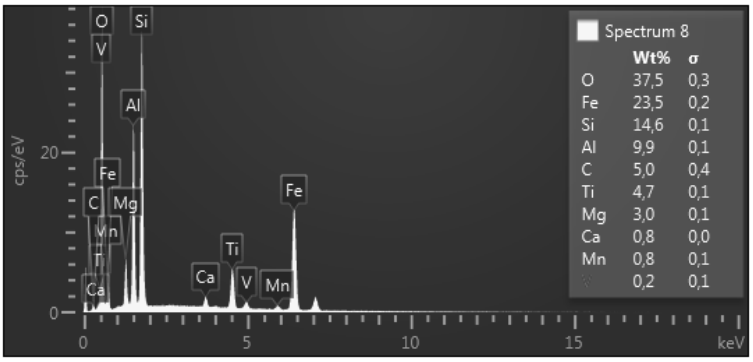

Figure 4.19: XEDS spectrum showing composition of abrasive particle from point analysis

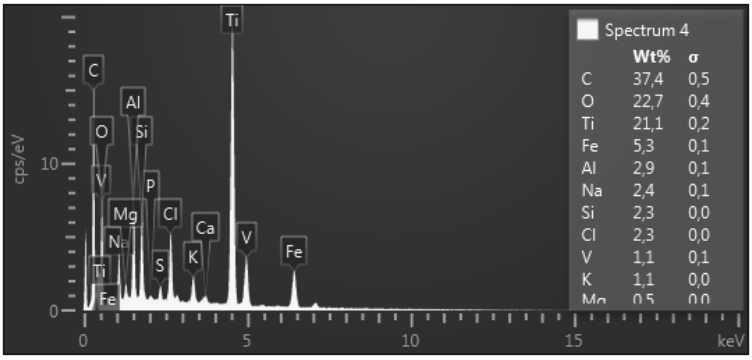

Figure 4.20: XEDS spectrum showing composition of organic particle from point analysis

5

Discussion

In this chapter, summary and discussion of the results are presented and possible errors are reviewed, in order to reach relevant conclusions.

5.1 Material Thickness

As proven by the results one of the most dominant factors in these experiments is the material thickness. Responses influenced by the thickness showed non-linear dependence. The range of dimensions selected for the experiments seemed too wide for proper evaluation of responses where parameter selection, based on the cutting of the thickest sheets, only resulted in measurable features in these samples. Although response modeling indicates high validity due to the selected material thicknesses, which might have decreased the relative significance of other factors. It should therefore be noted that the evaluation of other AWJ parameters would benefit from being examined for a certain thickness only.

Surface roughness was affected by material thickness. The jet becomes more unstable when cutting deeper into the material. Hence, this yields higher roughness on the kerf exit. For the same reason, the height of the rough cutting region should increase in thicker sheets. However, the striations could only be visualized for the thickest samples. Similarly, the lag and striation width may be affected in the same way.

There was a major effect of thickness on edge rounding diameter measured. This is not expected to be logical and was probably indicates measurement problems. The material thickness should not have any effect on edge rounding width, instead due to exposure caused by abrasive feed and cutting speed. Thickness might very well have had some minor effect on the depth of the edge rounding, however not as significant as indicated in the coefficient plot.

Taper angle was mainly affected by thickness. The model fit was very good for both standard and fine tests, with good residuals and replicates as well. The decrease of the taper angle in thicker material can be explained by the jets tendency to flatten in the traverse direction and creating a narrower kerf further down into the material. Potential cause of error could have been the measurement method, where small offsets relating to thicknesses may have resulted in the small angle difference.

5.2 Abrasive Feed Rate

The abrasive feed rate showed significant influence on edge rounding, where higher rate corresponds to rounder kerf entrance. This effect is mainly observed in standard AWJ; but also a smaller indication was seen for the fine AWJ process. The relation could have come from the higher amount of stray particles eroding and rounding off the initial deformation region in the vicinity of the kerf.

The effect of increasing abrasive flow on improving surface roughness citepshaw, as described in chapter 2.2.3, could to some extent be seen in the model (Figure F.13).

5.3 Water Pressure

Few significant influences from water pressure were revealed in the analysis. Improvements on surface finish or possibilities to increase traverse rate should be permitted by higher water pressures and may become more significant using wider range of the parameter. The observed, significant effect on striation lag might be thought as the particle curve due to deceleration in relation to traverse speed where the pressure correlates to the particle velocity, as previously stated in chapter 2.2.3. However, the factor may relate to responses outside the scope of this thesis. For instance, the influence from water pressure on the embedment of abrasive particles as shown by Boud et al. (2010), whereby higher pressure increases particle impact force and penetration depth. Evaluation of such can be important if removal of contamination is required.

5.4 Traverse Rate

The traverse rate influenced the responses complementarily to the material thickness, previously stated in chapter 2.2.3. Thus, thicker components can, to some extent, be cut with comparable quality to a thinner sheet if the traverse rate is lowered. This factor thus mainly affects responses corresponding to the surface roughness, namely jet lag, striation width, height of the RCR and surface roughness.

Presumably the influence of increasing abrasive feed rate could be projected onto a slower cutting speed, where more abrasive particles erode a certain distance of the kerf. Consequently, lower speed should result in more edge rounding.

5.5 Abrasive Grit Size

There seems to be an effect of grit size on edge rounding in FAWJ, where larger grains cause more rounding. There are no signs of this for standard AWJ. This might be due to the grit size relative to the jet diameter, as defects generated in FAWJ could display features of individual particles rather than the area of the jet.

5.6 Abrasive Grit Type

Though not intended, variations occurred in abrasives used in the conducted experiments.

Recycled sand is as mentioned rounder than fresh abrasive particles. One of the three sand types used in the FAWJ was recycled and exhibited rounder shape, which can be seen in Figure 5.1. This might have caused the higher feed rate compared to the other sands (refer to J.1, verification of abrasive feed rate). The effects of sand type on cutting performance are disputed. According to Boud et al. (2010), there are no difference in cutting efficiency and grit embedment. Furthermore, the morphology of embedded particles, which could affect mechanical properties of the cut product, is not determined by initial shape since particles likely shatter on impact. Additionally, recycled sand might contain other elements from previous cutting, which may or may not be detrimental from a contamination perspective.

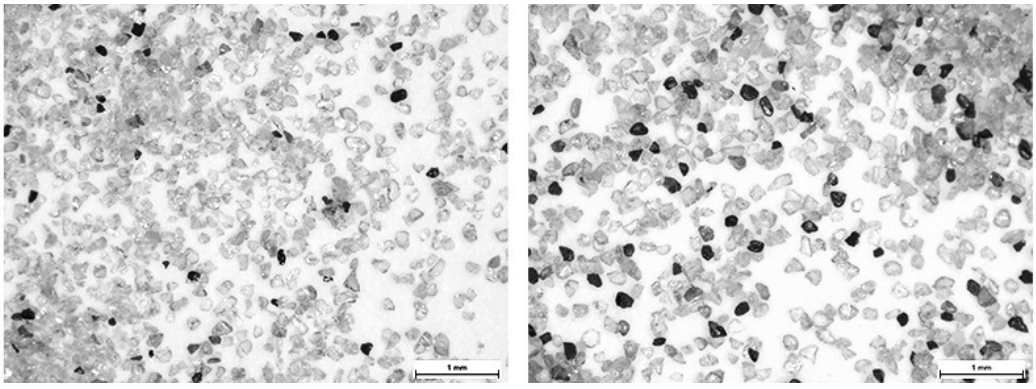

Figure 5.1: Comparison image of the differing morphology of abrasive grains in 20x magnification, 200 mesh recycled sand to the left and 150 mesh non-recycled abrasives to the right

5.7 Grit Embedment

Silicon was observed present in all investigated samples, however too few measurements were done to enable a rigid comparative analysis.

The initial deformation region and the face surrounding the kerf form a higher angle attack with the incident jet. The higher angle extend grit embedment with increased impact forces, concluded by Fowler, Pashby, and Shipway (2009)), and has further demonstrated higher concentrations of particles in IDR (Boud et al., 2010). Following this, the presence indicated from the XEDS analyses might be uneven with most particles situated in the top portion. This could be an interesting issue if removal of contaminated surface is considered.

The use of AWJ as a cutting method in aerospace applications is highly dependent on the effect of silicon containing residuals and other particles embedded in the

cut surface. Further research is required to investigate the effect of these particles when heated or when stressed in assemblage or service.

The entire extent to which the jet affects the kerf entrance side is not completely investigated and hence not clarified. There is sometimes a deformation zone due to stray particles outside the edge rounding area. This area could be prone to particle embedment, but was not investigated. It would require additional analysis, which was outside the scope of this project.

5.8 Note on burr

Inspected burrs were evidently broken off in many cases, see Figure 5.2, or curved away from the kerf which complicated evaluation. This deformation might be due to the handling. Although, burrs observed on samples were small (see Table 4.2). Since basically no heat input during the process is present, no hardening of burrs should have occurred. There has been no further investigation regarding possible impact on deformation hardening of the burr.

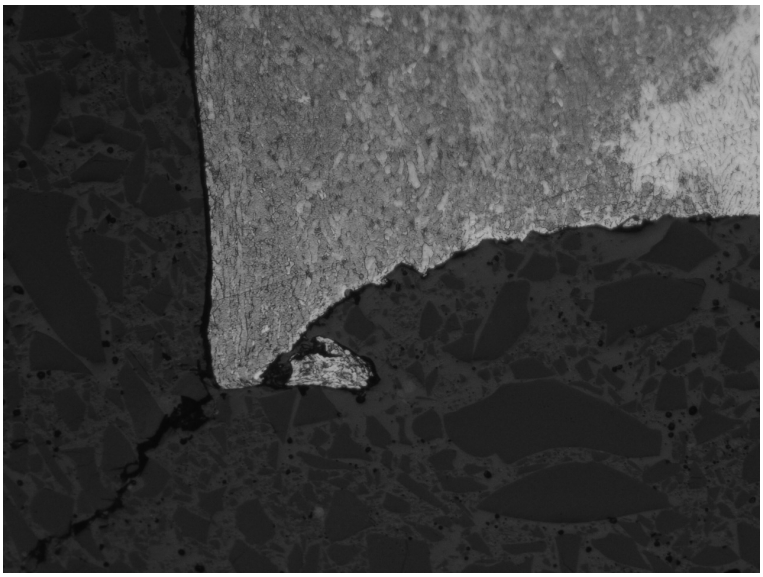

Figure 5.2: Broken off burr

5.9 Extra Tests

The extra tests performed were not evaluated due to time constraints. These tests were not performed to provide a full factorial setup, and will not yield a complete process window. Complementing parameters will have to be performed to achieve this. Otherwise, analysis of those specific parameters can be done individually.

5.10 Uncertainties and Error Sources

Before making conclusions from results, sources of errors should be considered. While the influence of some recognized uncertainties could be evaded or minimized, others were revealed after the execution of experiments, sample preparation or evaluation. Thus being aware of such is necessary for proper interpretation.

5.10.1 Experimental Setup

The mounting in both FAWJ and AWJ processes used clamping to secure the workpiece and prevent flexing. While AWJ used a rigid grating supporting the processed sheets, the material in FAWJ is mounted circumferentially. However, the larger diameter jet in AWJ applies more force and was observed to curve the material occasionally which could create irregularities and geometrical defects. In addition, the jets interaction with the support grating could be responsible for periodic features because of jet rebound.

Humidity rises during the day, which could have affected abrasive feed rate in the experiments. However, the extent to which this affected the tests was probably negligible, as the center points which were done during different times of the day did not show any distinct error.

The pump supplied the nozzle with variable pressure. The observed deviation was in the range of hundreds of bar for AWJ and less for FAWJ around the calibrated value.

5.10.2 Preparation of Samples

Samples have been fixed into bakelite holders where the flatness of each piece varies, which can result in deviations in observed geometries. Greatest impact should be in the finer cuts where it might transcend the actual process parameter dependencies. Evidence of such effect may be the fact that different sheet thicknesses were measured throughout studies of transverse sections.

The grinding and polishing of longitudinal sections followed the predetermined instruction of abrasive to use and time for each step. However, some differences were to be expected where the result being variances in sectional depth at which subsequent measurements were conducted.

The depth achieved by grinding the longitudinal samples varied depending on sheet thickness since surface defects from sheet rolling had to be removed and these were larger on the thicker samples. The method of removing 10 % of the thickness was sufficiently to avoid the defects but resulted in depth variations when surface roughness was analyzed. Additionally the procedure was based on specified sheet thicknesses, which in subsequent measurements proved to be inaccurate (chapter 3.8).

The aim was to keep the sample holders six positions fully occupied during polishing and grinding to enable uniform material removal rates and conditions. However this was not possible through the whole specimen series because of uneven numbers in the separated groups of samples. Towards the end of each session, samples were divided to leave equal and least amount of vacancies.

5.10.3 Geometrical measurements

In visual inspection, variations in the measurements can consist of multiple persons doing the measuring, calibrations and differences between equipment used.

An effort to minimize the impact of measurement differences was planed where the inspections were conducted in pair and followed the established courses of action. Calibration of the equipment was affirmed before each inspection with reassessment of samples to verify similar method of measurement.

When calculating averages from measured responses the position of the sample in the component should be considered. Some pieces might have been more suitable for conclusions since velocity ramping in geometries could have affected the process experienced by the material. As the ramping was depending on longitudinal position, so were the studied samples. However, there was no noticeable difference in section a, which was in a ramping area, compared to piece b and c in the test samples.

Measuring at the same magnification for comparability posed difficulties in accuracy especially for samples produced with the fine process. The dimension of the thickest samples limited the geometrical measurements to be performed at low magnification. This resulted in low precision of the related responses and thus derived results should be considered accordingly.

Furthermore, low magnification led to difficulties in evaluating taper of thinner samples and thus measurements of the thicker sections may take precedence in analysis.

Also, measurement on rounded edges in the kerf entrance proved to be difficult. To distinguish taper from edge roundness the corners were zoomed in on the thinner sheet tests which may have resulted in response artifacts. Hence, to redo measurements of edge roundness at higher magnification, e.g. 200x, might feature higher accuracy yet evidently some samples were deformed (Figure 5.3) due to adverse process variables.

Measurements on arched burr (Figure 3.6) could have been inaccurate because of the straight line ruler in the software. Traces of chipped off burr in the plastic mounted samples and folded edges hindered the measurements for some samples.

Studies of striations where disregarded in test pieces absent of jet lag. The features of striations in these samples ought to be better evaluated through surface

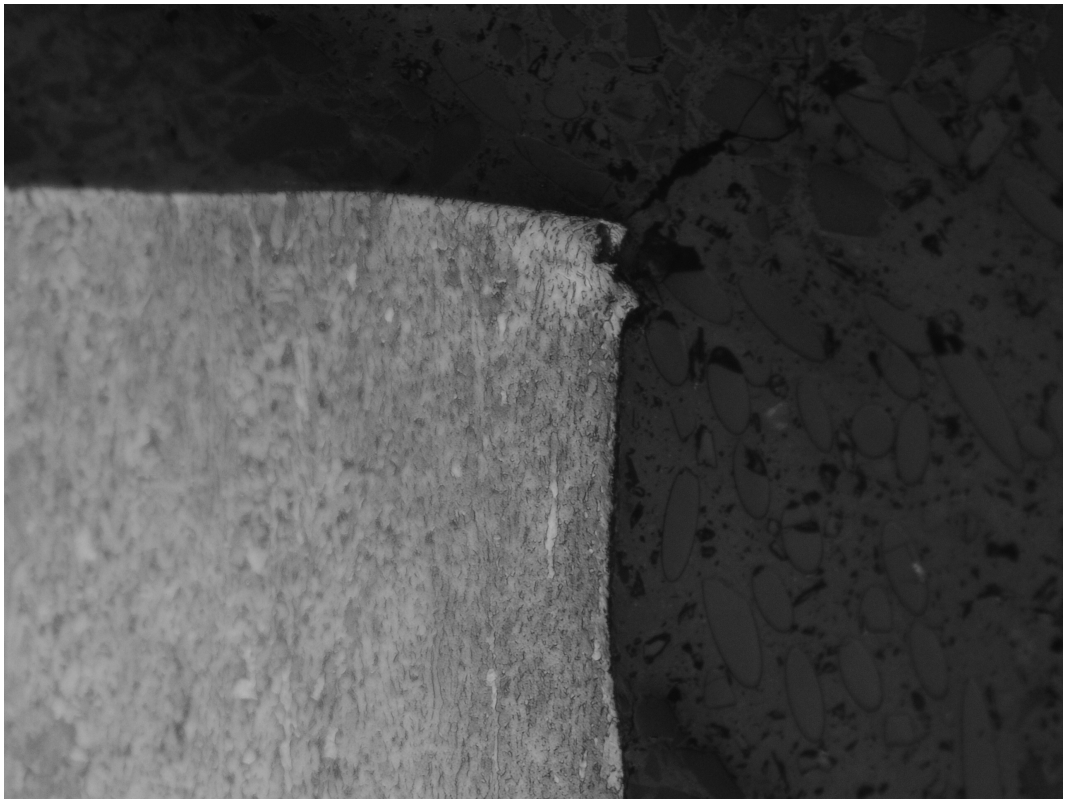

Figure 5.3: Large defect in the kerf entrance, complicating measurements of edge rounding

roughness test.

5.10.4 Chemical Analysis

Since samples analyzed in SEM did not undergo the sample preparations like the polished and etched sections used in other evaluations, the handling of samples may be responsible for anomalies in chemical analysis. The observed high carbon content, appearing in dark spots throughout the samples, was most likely a result of dirt or grease as as these spots were removed by ultrasonic washing. Cleaning of samples did, however, not result in significant difference of XEDS analysis results. The only difference was the apparent decrease in measured carbon by 5 wt% carbon after the cleaning, compare Figures G.8 and G.9 in Appendix G.

The XEDS mapping for quantitative analysis was not large enough to cover the entire area of the 6.35 mm sample from top to bottom, from jet entrance to exit. This means that not all three regions (IDR, SCR and RCR) were covered equally, and this might cause a deviation in the result compared to the other two sheet thicknesses.

5.10.5 Wear on Test Equipment

During testing the focus tube gets worn. This, increases the affected area on the work piece as well as other factors (chapter 2.2.3). The effect was not well known or monitored, but may be assumed as insignificant as the center points samples were not deviating much throughout the day, which would be the case if tool wear would have had large impact. Furthermore, the focus tube was replaced before the experiment and should not have experienced any significant wear during the tests.

5.10.6 Comments Regarding Statistical Analysis

Regarding the performed analysis in Modde, further work could be done to create better models. One example is the consideration of how other non-linear factors affect the resulting parameters.

6
Conclusions

Some important parameters affecting the result of the abrasive waterjet process have been concluded from the results. Additionally suggestions on how the study might continue are presented. The results were mainly corresponding to expectations and previous research, further reinforcing the knowledge of AWJ. However, there were some inconclusive uncertainties found as well, which requires more affirmation to conclude whether they were measuring errors or not.

6.1 Main Factors of AWJ and FAWJ Processes

- The two main factors affecting result parameters were sheet thickness and traverse rate. They affected surface finish (jet lag, striation width, height of rough cutting region and surface waviness), with a direct proportionality. The relations observed correlated with previous work presented in chapter 2.2.3. Contour plots confirmed the behavior and the coupling between the factors.
- Taper angle was mainly affected by plate thickness according to the statistical analysis, with an inverse proportionality. The cause of this may be the flattening of the jet further down into the material. Refer to the discussion in chapter 5.1.
- Edge rounding was observed to be proportionally affected by abrasive feed rate.
- The results indicate that larger grit size causes more edge rounding in FAWJ processing.
- Silicon was found in all nine samples investigated in the XEDS analysis. This indicates that there are residual abrasive particles left in the kerf. Although not proven from the analyses, it is supposed that the presence of these particles may be concentrated around the kerf entrance according to Boud et al. (2010).
- No significant burrs are produced from AWJ cutting and their removal should be trivial.

6.2 Suggestions for Further Studies

During analysis of the results, many topics and areas for further studies were identified.

Regarding the particle embedment, performing of SEM analysis in the IDR separately is motivated, as there might be a higher degree of particle embedment here. Also, testing for residual silicon on milled and Si-C ground components in order to compare with AWJ cut components, could give insight on tolerable silicon containing residuals on the cut titanium parts.

Testing wider parameters ranges is recommended to see if further improvements are possible. Such parameters could be standard AWJ with higher pressures (above 6000 bar) and lower cutting speed in both AWJ and FAWJ. Further tests on fixed material thickness for statistical evaluation of parameter influence is supposed to be important, since results on thinner samples generated too small defects for the method of measurement and lack of input for modeling in software. This might make the effects of process parameters clearer.

Regarding areas for continued analysis, cost calculations for cutting time vs. adding an additional step might be interesting, to determine financial incentive. Additionally, measuring the jet affected zone outside the edge rounding area and investigating its eventual particle embedment is of concern. This deformation was not considered in this thesis study, but was a noticeable effect from the cutting process. The analysis in Modde could be taken further with more elaborate use of its capabilities with respect to such as non-linear correlations, possibly yielding better models.

The extra tests performed were not evaluated due to time constraints, but they could provide useful insight on higher speed cutting if investigated further.

Some methods of evaluation of the result parameters were not ideal. This has been discussed in chapter 5. For example, defects from cutting made certain geometries hard to distinguish and thereby hard to measure.

Bibliography

M. Ramulu, Seo Y.W., M. Hashish, P. Pedersen, and P. Posinasetti. Cutting characteristics of titanium alloy by abrasive waterjet. In Paul Lake, editor, *16th International Conference on Water Jetting*, pages 201–210. BHR Group Limited, Aix-en-Provence, 2002.

R.N. Caron and J.T. Staley. Titanium and titanium alloys. In Paul Lake, editor, *ASM Handbook Processing, and Structure on Properties of Nonferrous Alloys*, volume 20, page 383–415. ASM International, 1997.

Christian Öjmertz. *A Guide to: Waterjet Technology*. Institutionen för Produktionsteknik Chalmers Tekniska Högskola, Göteborg, 1994.

G.A. Mort. Results of abrasive water jet market survey. In Paul Lake, editor, *Proceeding of the 8th American Water Jet Conference*, pages 259–282, 1995.

M. C. Shaw. *Principles of Abrasive Processing*. Oxford University Press Inc., New York, 1996.

M Allaby. *Dictionary of Earth Sciences (3rd Edition)*. Oxford University Press, 2008.

J.E. Kogel, N.C. Trivedi, J.M. Barker, and S.T Krukowski. *Industrial Minerals and Rocks - Commodities, Markets, and Uses (7th Edition)*, page 151. Society for Mining, Metallurgy, and Exploration, 2006.

Christian Öjmertz. *SWA Snittnorm*. Swedish Waterjet Association, 2004.

D.K. Shanmugam, J. Wang, and H. Liu. Minimisation of kerf tapers in abrasive waterjet machining of alumina ceramics using a compensation technique. In *International Journal of Machine Tools and Manufacture*, pages 1527–1534. Elsevier B.V., 2008.

J Zeng and J.T. Kim. Parameter prediction and cost analysis in abrasive waterjet cutting operations. In *7th American Water Jet Conference*, Seattle, 1993. Water Jet Technology Association.

F. Boud, C. Carpenter, J. Folkes, and P. H. Shipway. Abrasive waterjet cutting of a titanium alloy: The influence of abrasive morphology and machnical properties on work piece grit embedment and cut quality. In *Journal of Materials Processing Technology*, pages 2197–2205. Elsevier B.V., 2010.

W.Y. Li, J. Wang, and Y.M. Ali. An experimental study of radial-mode abrasive waterjet turning of steel. In *Advances in Materials Manufacturing Science and Technology XIV*, pages 465–489. Trans Tech Publications, Switzerland, 2011.

D.S. Miller. Micromachining with abrasive waterjets. In Paul Lake, editor, *16th International Conference on Water Jetting*, pages 59–74. BHR Group Limited, Aix-en-Provence, 2002.

S. Wold, J. Trygg, A. Berglund, and H. Antti. Some recent developments in pls modeling. In *Chemometrics and Intelligent Laboratory Systems 58*, pages 131–150. Elsevier B.V., 2001.

S. Bisgaard and M. Kulahci. Quality quandaries: The application of principal component analysis for process monitoring. In *Quality Engineering 18*, pages 95–103. Taylor & Francis, 2006.

G. Fowler, I. R. Pashby, and P. H. Shipway. The effect of particle hardness and shape when abrasive water jet milling titanium alloy ti6al4v. In *Wear*, pages 613–620. Elsevier B.V., 2009.

A

Test Plan

Table A.1: Test Plan Traditonal AWJ

Experiment	Run Order	Thickness	Water Pressure	Abrasive Feed	Traverse Rate	Abrasive Grit Size	Position
1	1	1	3000	250	100	80	1
10	2	6.35	3000	250	300	80	1
32	3	6.35	4000	500	300	120	2
21	4	1	4000	250	100	120	2
29	5	1	4000	250	300	120	3
36	6	3.2	3500	375	200	100	1 and 2
37	7	3.2	3500	375	200	100	3
8	8	6.35	4000	500	100	80	5
6	9	6.35	4000	250	100	80	6
24	10	6.35	4000	500	100	120	7
30	11	6.35	4000	250	300	120	8
26	12	6.35	3000	250	300	120	9
2	13	6.35	3000	250	100	80	10
11	14	1	3000	500	300	80	4
33	15	3.2	3500	375	200	100	4
34	16	3.2	3500	375	200	100	5
27	17	1	3000	500	300	120	7
23	18	1	4000	500	100	120	8
15	19	1	4000	500	300	80	9
4	20	6.35	3000	500	100	80	11
12	21	6.35	3000	500	300	80	12
25	22	1	3000	250	300	120	10
19	23	1	3000	500	100	120	11
28	24	6.35	3000	500	300	120	14
9	25	1	3000	250	300	80	12
14	26	6.35	4000	250	300	80	15
3	27	1	3000	500	100	80	13
5	28	1	4000	250	100	80	14
31	29	1	4000	500	300	120	15
17	30	1	3000	250	100	120	16
20	31	6.35	3000	500	100	120	16
13	32	1	4000	250	300	80	17
16	33	6.35	4000	500	300	80	17
7	34	1	4000	500	100	80	18
18	35	6.35	3000	250	100	120	18
22	36	6.35	4000	250	100	120	19
35	37	3.2	3500	375	200	100	6

Table A.2: Test Plan Traditonal AWJ - Additional Tests

Experiment	Run Order	Thickness	Water Pressure	Abrasive Feed	Traverse Rate	Abrasive Grit Size	Position
38	38	6.35	3500	375	500	100	20
39	39	6.35	3500	375	750	100	21
40	40	3.2	3500	375	500	100	7
41	41	3.2	3500	375	750	100	8
42	42	3.2	3500	375	1000	100	9
43	43	3.2	3500	375	1250	100	10
44	44	3.2	3500	375	1500	100	11
45	45	1	3500	375	500	100	19
46	46	1	3500	375	750	100	20
47	47	1	3500	375	1000	100	21
48	48	1	3500	375	1250	100	22
49	49	1	3500	375	1500	100	23

Table A.3: Test Plan Micro AWJ

Experiment	Run Order	Thickness	Water Pressure	Abrasive Feed	Traverse Rate	Abrasive Grit Size	Position
34	1	3.2	3500	20	45	200	13
36	2	3.2	3500	20	45	200	14
7	3	1	4000	25	30	150	24
11	4	1	3000	25	60	150	25
1	5	1	3000	15	30	150	26
13	6	1	4000	15	60	150	27
9	7	1	3000	15	60	150	28
15	8	1	4000	25	60	150	29
3	9	1	3000	25	30	150	30
5	10	1	4000	15	30	150	31
6	11	6.35	4000	15	30	150	22
16	12	6.35	4000	25	60	150	23
12	13	6.35	3000	25	60	150	24
8	14	6.35	4000	25	30	150	25
4	15	6.35	3000	25	30	150	26
14	16	6.35	4000	15	60	150	27
10	17	6.35	3000	15	60	150	28
2	18	6.35	3000	15	30	150	29
33	19	3.2	3500	20	45	200	15
37	20	3.2	3500	20	45	200	16
19	21	1	3000	25	30	230	32
25	22	1	3000	15	60	230	33
27	23	1	3000	25	60	230	34
17	24	1	3000	15	30	230	35
31	25	1	4000	25	60	230	36
29	26	1	4000	15	60	230	37
23	27	1	4000	25	30	230	38
21	28	1	4000	15	30	230	39
30	29	6.35	4000	15	60	230	30
28	30	6.35	3000	25	60	230	31
20	31	6.35	3000	25	30	230	32
26	32	6.35	3000	15	60	230	33
18	33	6.35	3000	15	30	230	34
24	34	6.35	4000	25	30	230	35
32	35	6.35	4000	25	60	230	37
22	36	6.35	4000	15	30	230	38
35	37	3.2	3500	20	45	200	17

B

Test Equipment

B.1 AWJ Setup

Table B.1: Test setup for AWJ

Water cutting machine	Information missing
Volts/Phase/Hz	-/-/-
Max water pressure	-
Pump	-
Working pressure	-
Max. flow rate	-
CNC	-

B.2 FAWJ Setup

(BILD)

Table B.2: Test setup for FAWJ

Water cutting machine	NCM 10
Volts/Phase/Hz	400/3/50
Max water pressure	4136 bar
Pump	HYTRON 40.37
Working pressure	400 bar
Max. flow rate	3.8 l/min
CNC	FANUC series 31i MODEL A

C

Abrasive specifications

Table C.1: Specifications of abrasives used in standard AWJ experiment

Grit size	Abrasive	Manufacturer	Note
80 mesh	supergarnet	AMPECO GmbH	
100 mesh	supergarnet	AMPECO GmbH	E+*
120 mesh	supergarnet	AMPECO GmbH	

* *Quality E+ is supposed to equal 100 mesh according to supplier.*

Table C.2: Specifications of abrasives used in FAWJ experiment

Grit size	Abrasive	Manufacturer	Note
150 mesh	GMA 150 GMRD	GMA Garnet	
200 mesh	GMA 200	GMA Garnet	Recycled
230 mesh	Barton HPX 230	Barton International	

D

Response Sheets

The data in this chapter have been excluded from this version of the report, due to the secrecy of company property. The tables below features the response data from analysis.

Table D.1: Response Sheet Standard AWJ

Exp	n	n_r	f	f_r	h_R	h_{R_r}	a	u	w_r	h_r	d_r	w_b	l_b	β	r_z	$r_z r$
1	-	-	-	-	-	-	-	-	-	-	-	-	-	-	-	-
2	-	-	-	-	-	-	-	-	-	-	-	-	-	-	-	-
3	-	-	-	-	-	-	-	-	-	-	-	-	-	-	-	-
4	-	-	-	-	-	-	-	-	-	-	-	-	-	-	-	-
5	-	-	-	-	-	-	-	-	-	-	-	-	-	-	-	-
6	-	-	-	-	-	-	-	-	-	-	-	-	-	-	-	-
7	-	-	-	-	-	-	-	-	-	-	-	-	-	-	-	-
8	-	-	-	-	-	-	-	-	-	-	-	-	-	-	-	-
9	-	-	-	-	-	-	-	-	-	-	-	-	-	-	-	-
10	-	-	-	-	-	-	-	-	-	-	-	-	-	-	-	-
11	-	-	-	-	-	-	-	-	-	-	-	-	-	-	-	-
12	-	-	-	-	-	-	-	-	-	-	-	-	-	-	-	-
13	-	-	-	-	-	-	-	-	-	-	-	-	-	-	-	-
14	-	-	-	-	-	-	-	-	-	-	-	-	-	-	-	-
15	-	-	-	-	-	-	-	-	-	-	-	-	-	-	-	-
16	-	-	-	-	-	-	-	-	-	-	-	-	-	-	-	-
17	-	-	-	-	-	-	-	-	-	-	-	-	-	-	-	-
18	-	-	-	-	-	-	-	-	-	-	-	-	-	-	-	-
19	-	-	-	-	-	-	-	-	-	-	-	-	-	-	-	-
20	-	-	-	-	-	-	-	-	-	-	-	-	-	-	-	-
21	-	-	-	-	-	-	-	-	-	-	-	-	-	-	-	-
22	-	-	-	-	-	-	-	-	-	-	-	-	-	-	-	-
23	-	-	-	-	-	-	-	-	-	-	-	-	-	-	-	-
24	-	-	-	-	-	-	-	-	-	-	-	-	-	-	-	-
25	-	-	-	-	-	-	-	-	-	-	-	-	-	-	-	-
26	-	-	-	-	-	-	-	-	-	-	-	-	-	-	-	-
27	-	-	-	-	-	-	-	-	-	-	-	-	-	-	-	-
28	-	-	-	-	-	-	-	-	-	-	-	-	-	-	-	-
29	-	-	-	-	-	-	-	-	-	-	-	-	-	-	-	-
30	-	-	-	-	-	-	-	-	-	-	-	-	-	-	-	-
31	-	-	-	-	-	-	-	-	-	-	-	-	-	-	-	-
32	-	-	-	-	-	-	-	-	-	-	-	-	-	-	-	-
33	-	-	-	-	-	-	-	-	-	-	-	-	-	-	-	-
34	-	-	-	-	-	-	-	-	-	-	-	-	-	-	-	-
35	-	-	-	-	-	-	-	-	-	-	-	-	-	-	-	-
36	-	-	-	-	-	-	-	-	-	-	-	-	-	-	-	-
37	-	-	-	-	-	-	-	-	-	-	-	-	-	-	-	-

Table D.2: Response Sheet Fine AWJ

Exp	n	n_r	f	f_r	h_R	h_{R_r}	a	u	w_r	h_r	d_r	w_b	l_b	β	r_z	$r_z r$
1	-	-	-	-	-	-	-	-	-	-	-	-	-	-	-	-
2	-	-	-	-	-	-	-	-	-	-	-	-	-	-	-	-
3	-	-	-	-	-	-	-	-	-	-	-	-	-	-	-	-
4	-	-	-	-	-	-	-	-	-	-	-	-	-	-	-	-
5	-	-	-	-	-	-	-	-	-	-	-	-	-	-	-	-
6	-	-	-	-	-	-	-	-	-	-	-	-	-	-	-	-
7	-	-	-	-	-	-	-	-	-	-	-	-	-	-	-	-
8	-	-	-	-	-	-	-	-	-	-	-	-	-	-	-	-
9	-	-	-	-	-	-	-	-	-	-	-	-	-	-	-	-
10	-	-	-	-	-	-	-	-	-	-	-	-	-	-	-	-
11	-	-	-	-	-	-	-	-	-	-	-	-	-	-	-	-
12	-	-	-	-	-	-	-	-	-	-	-	-	-	-	-	-
13	-	-	-	-	-	-	-	-	-	-	-	-	-	-	-	-
14	-	-	-	-	-	-	-	-	-	-	-	-	-	-	-	-
15	-	-	-	-	-	-	-	-	-	-	-	-	-	-	-	-
16	-	-	-	-	-	-	-	-	-	-	-	-	-	-	-	-
17	-	-	-	-	-	-	-	-	-	-	-	-	-	-	-	-
18	-	-	-	-	-	-	-	-	-	-	-	-	-	-	-	-
19	-	-	-	-	-	-	-	-	-	-	-	-	-	-	-	-
20	-	-	-	-	-	-	-	-	-	-	-	-	-	-	-	-
21	-	-	-	-	-	-	-	-	-	-	-	-	-	-	-	-
22	-	-	-	-	-	-	-	-	-	-	-	-	-	-	-	-
23	-	-	-	-	-	-	-	-	-	-	-	-	-	-	-	-
24	-	-	-	-	-	-	-	-	-	-	-	-	-	-	-	-
25	-	-	-	-	-	-	-	-	-	-	-	-	-	-	-	-
26	-	-	-	-	-	-	-	-	-	-	-	-	-	-	-	-
27	-	-	-	-	-	-	-	-	-	-	-	-	-	-	-	-
28	-	-	-	-	-	-	-	-	-	-	-	-	-	-	-	-
29	-	-	-	-	-	-	-	-	-	-	-	-	-	-	-	-
30	-	-	-	-	-	-	-	-	-	-	-	-	-	-	-	-
31	-	-	-	-	-	-	-	-	-	-	-	-	-	-	-	-
32	-	-	-	-	-	-	-	-	-	-	-	-	-	-	-	-
33	-	-	-	-	-	-	-	-	-	-	-	-	-	-	-	-
34	-	-	-	-	-	-	-	-	-	-	-	-	-	-	-	-
35	-	-	-	-	-	-	-	-	-	-	-	-	-	-	-	-
36	-	-	-	-	-	-	-	-	-	-	-	-	-	-	-	-
37	-	-	-	-	-	-	-	-	-	-	-	-	-	-	-	-

E

Model Statistics Overview for Standard AWJ Samples

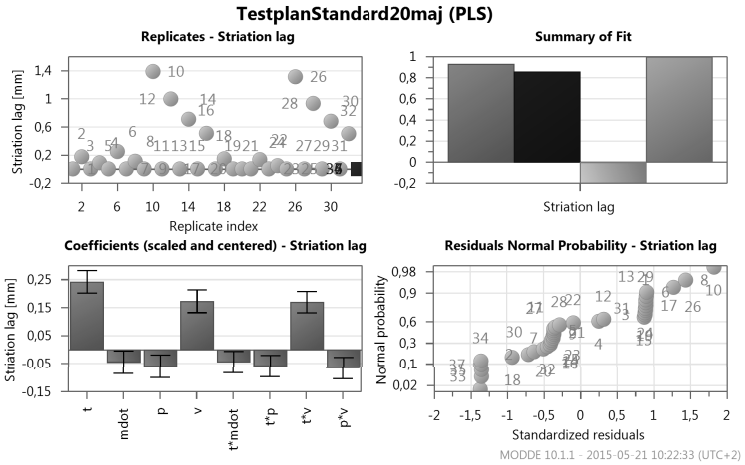

Figure E.1: Model statistics overview for striation lag (Standard AWJ)

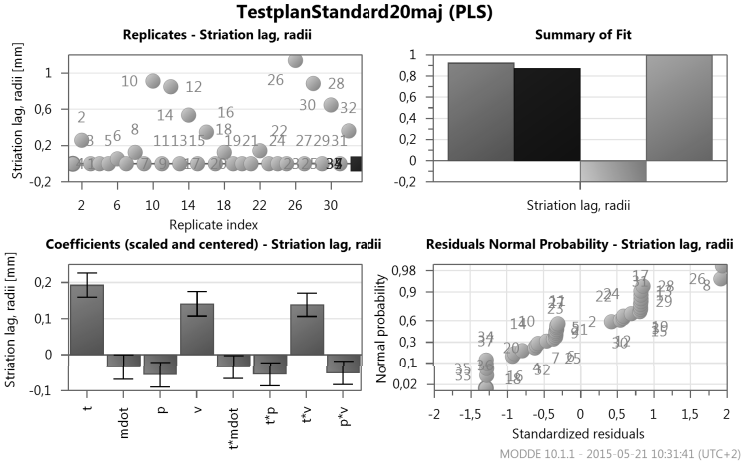

Figure E.2: Model statistics overview for striation lag in radii(Standard AWJ)

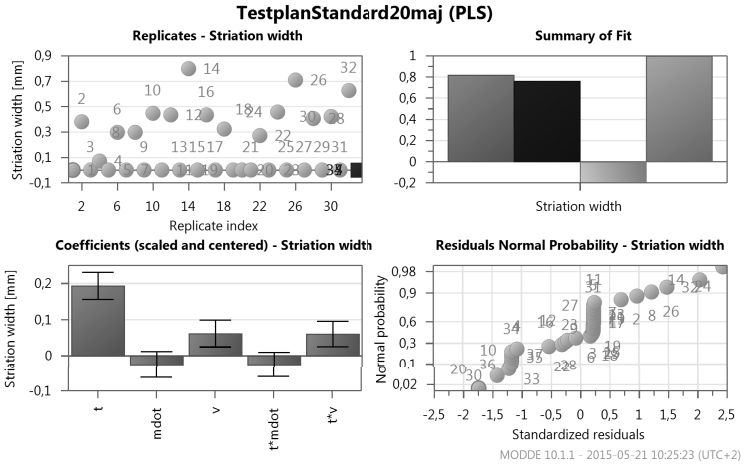

Figure E.3: Model statistics overview for striation width (Standard AWJ)

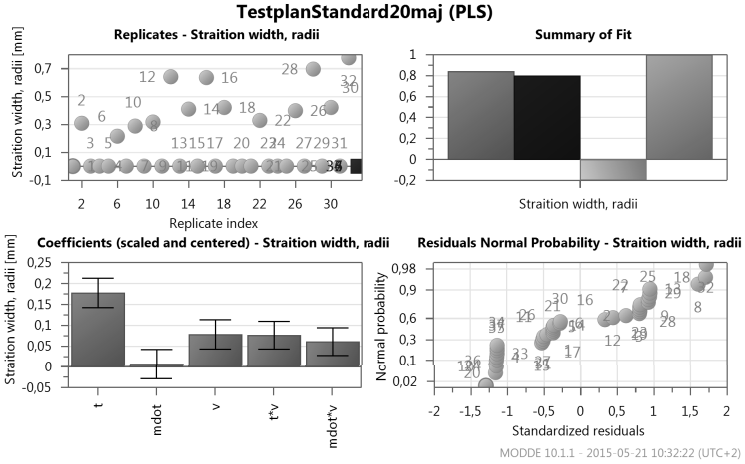

Figure E.4: Model statistics overview for striation width in radii (Standard AWJ)

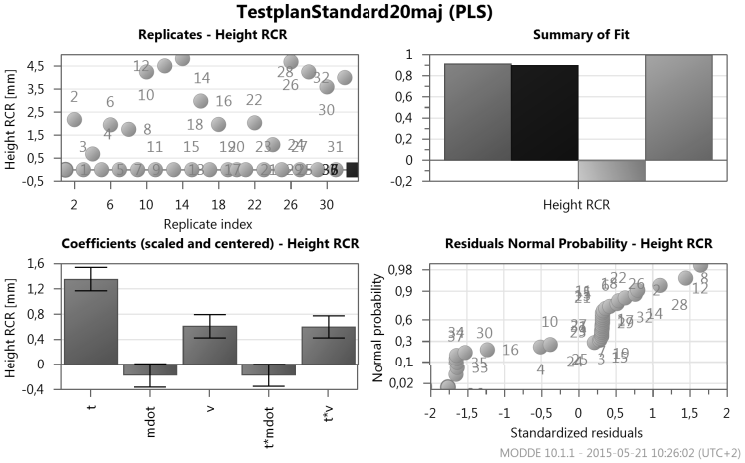

Figure E.5: Model statistics overview for RCR height (Standard AWJ)

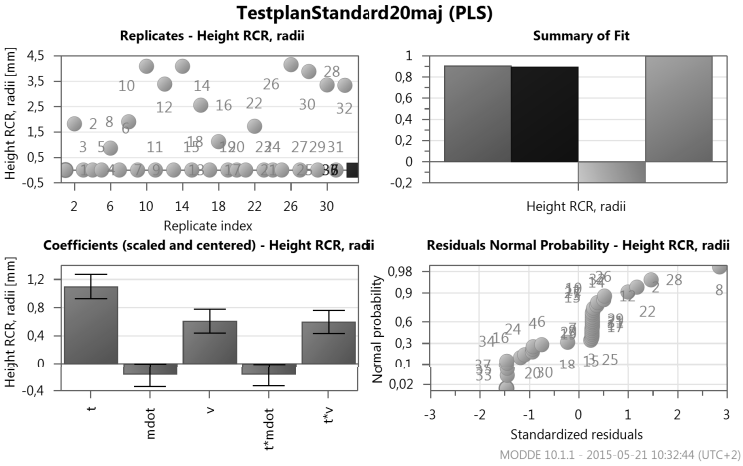

Figure E.6: Model statistics overview for RCR height in radii (Standard AWJ)

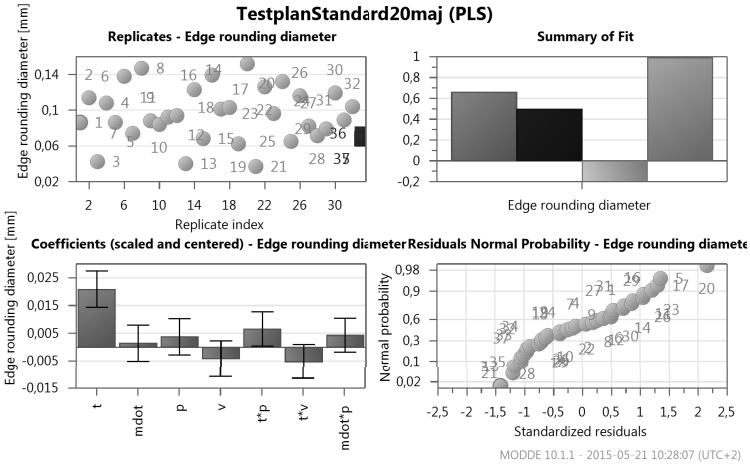

Figure E.7: Model statistics overview for edge rounding diameter (Standard AWJ)

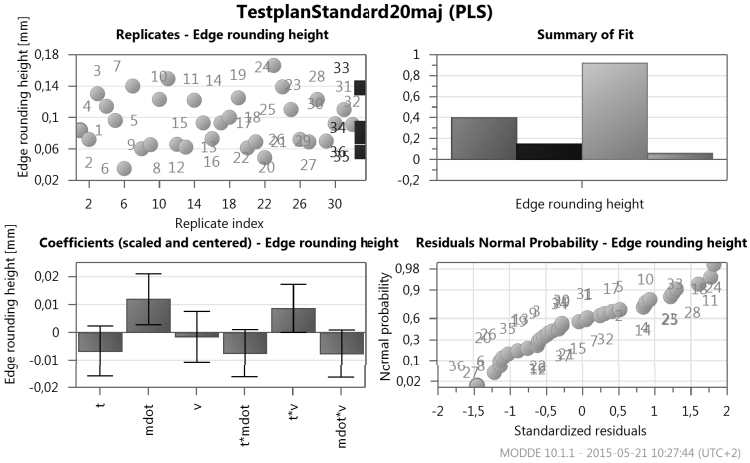

Figure E.8: Model statistics overview for edge rounding height (Standard AWJ)

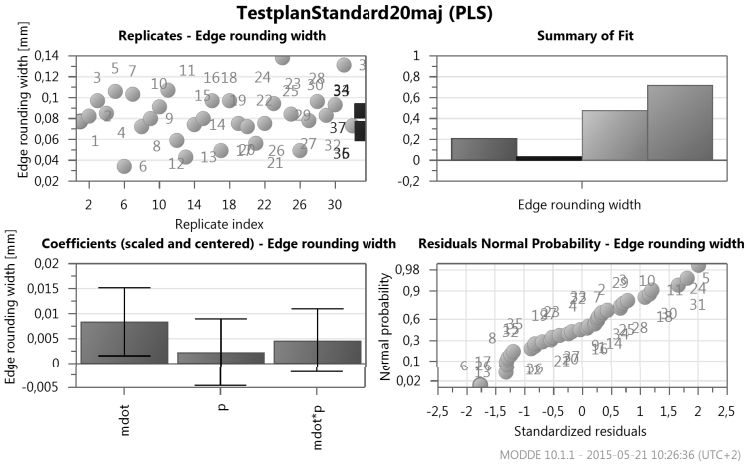

Figure E.9: Model statistics overview for edge rounding width (Standard AWJ)

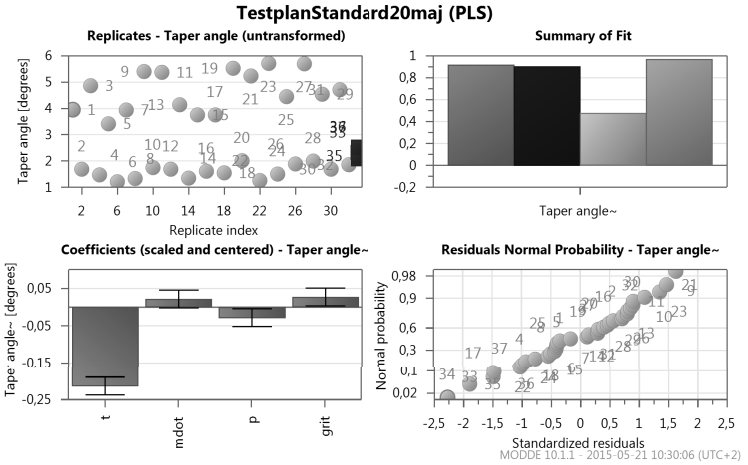

Figure E.10: Model statistics overview for taper angle (Standard AWJ)

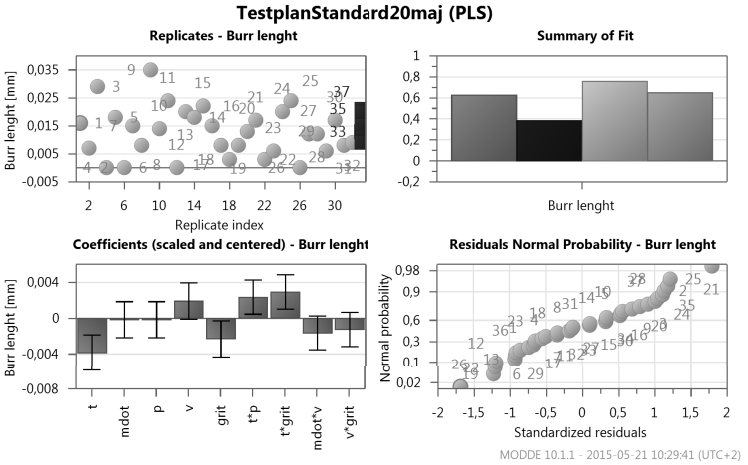

Figure E.11: Model statistics overview for burr length (Standard AWJ)

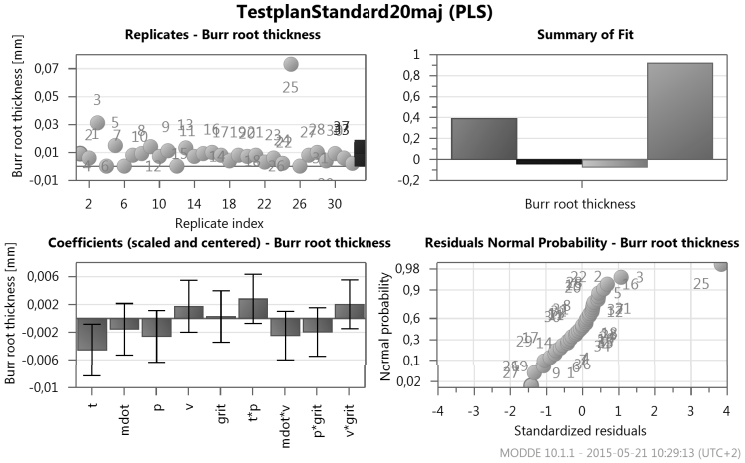

Figure E.12: Model statistics overview for burr root thickness (Standard AWJ)

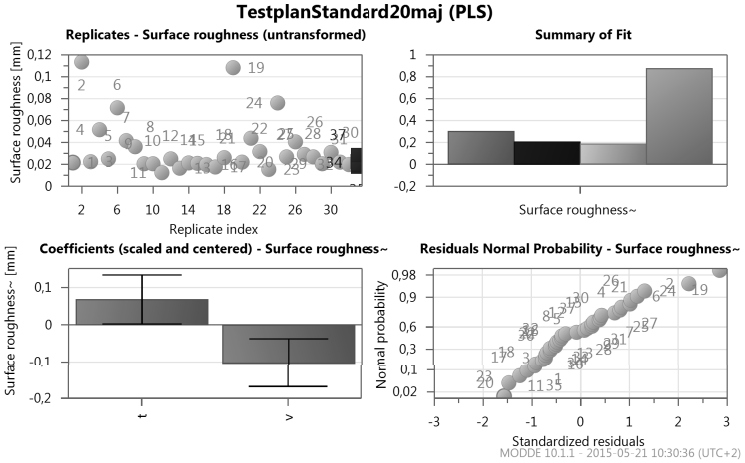

Figure E.13: Model statistics overview for surface roughness (Standard AWJ)

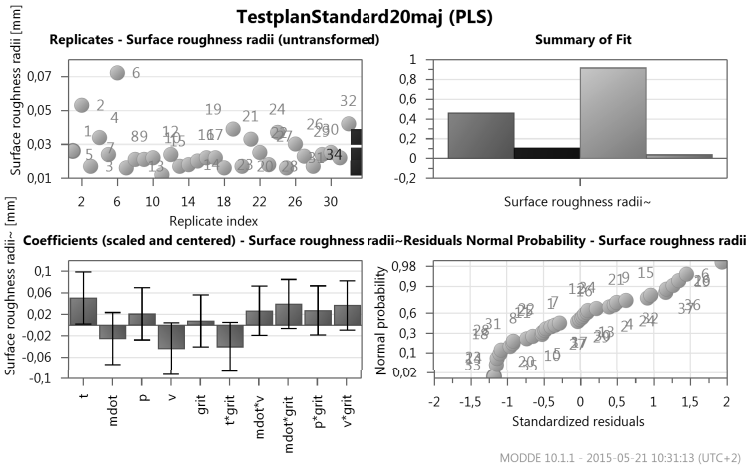

Figure E.14: Model statistics overview for surface roughness in radii (Standard AWJ)

F

Model Statistics Overview for FAWJ Samples

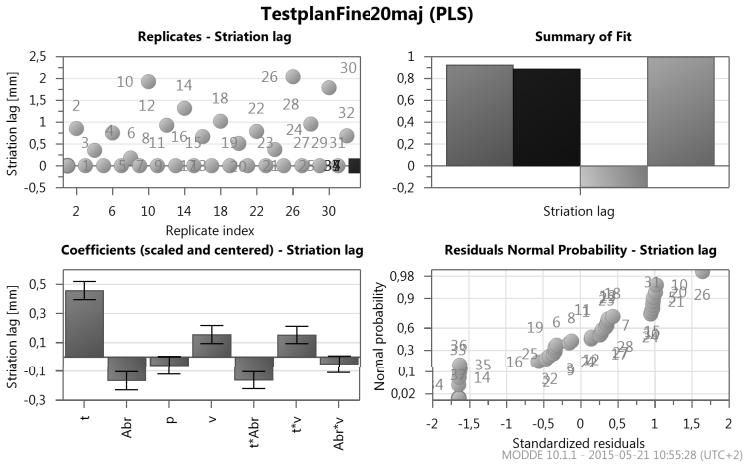

Figure F.1: Model statistics overview for striation lag (FAWJ)

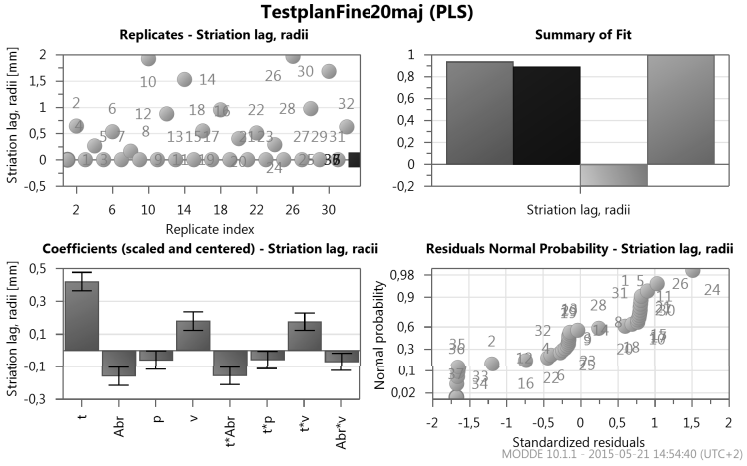

Figure F.2: Model statistics overview for striation lag in radii(FAWJ)

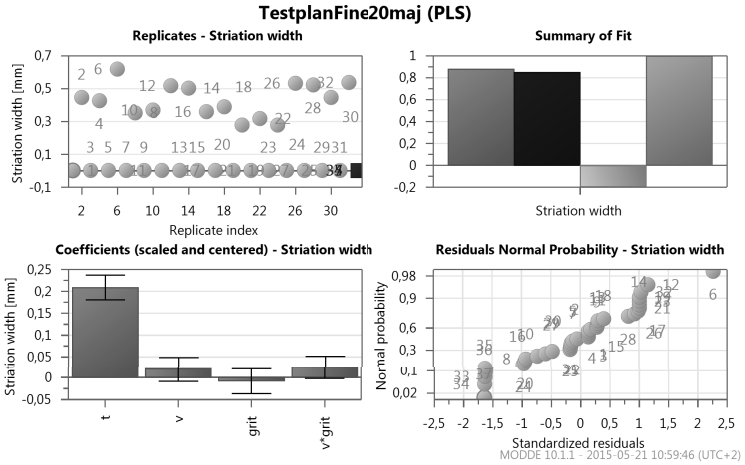

Figure F.3: Model statistics overview for striation width (FAWJ)

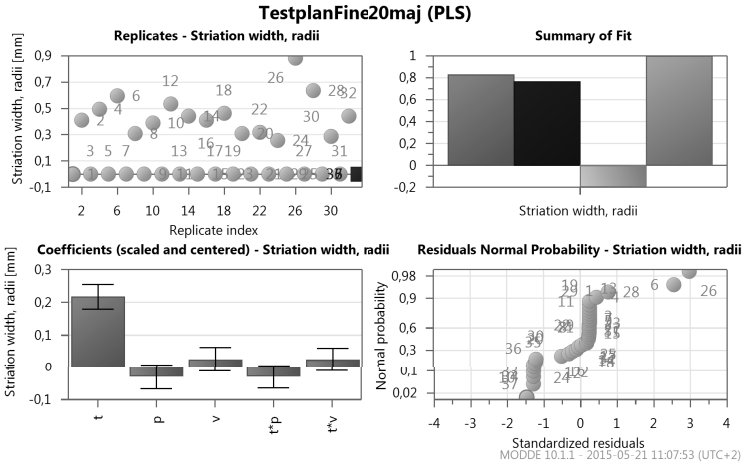

Figure F.4: Model statistics overview for striation width in radii (FAWJ)

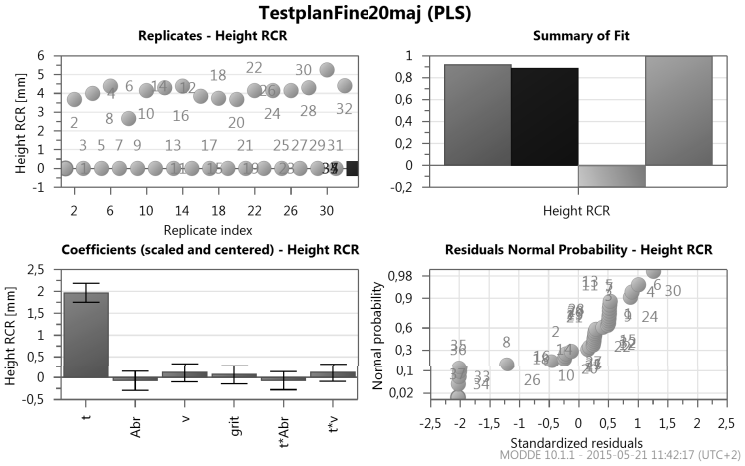

Figure F.5: Model statistics overview for RCR height (FAWJ)

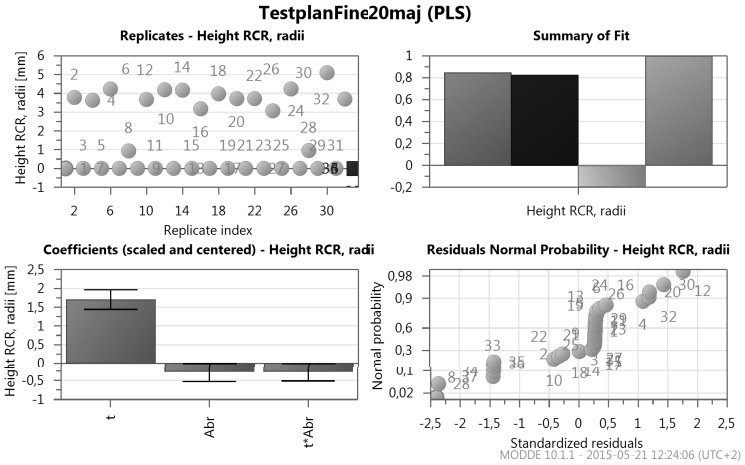

Figure F.6: Model statistics overview for RCR height in radii (FAWJ)

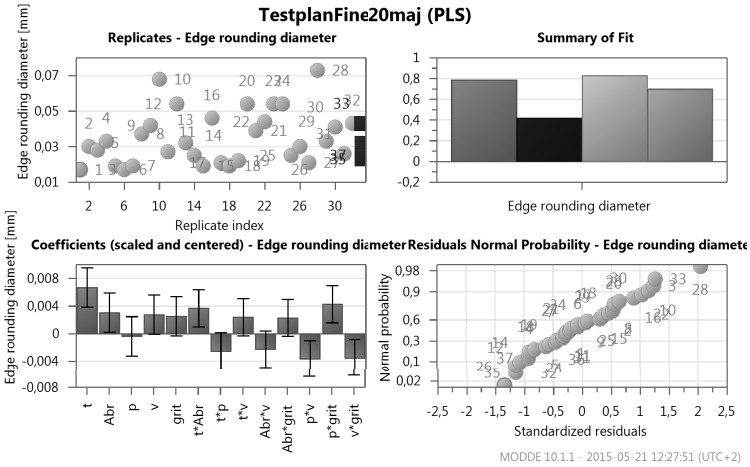

Figure F.7: Model statistics overview for edge rounding diameter (FAWJ)

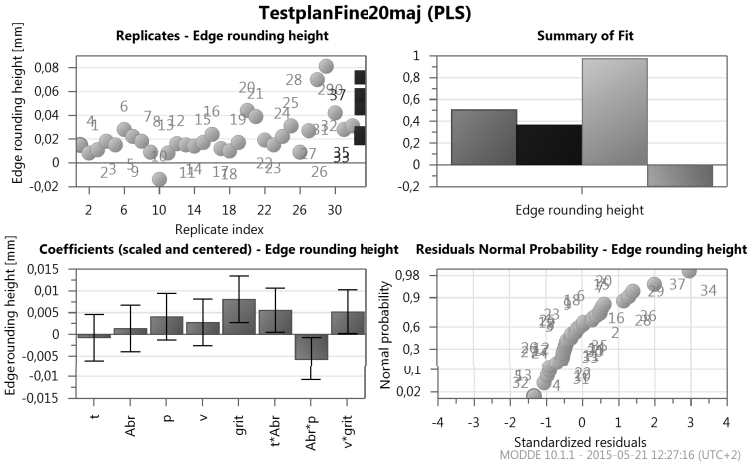

Figure F.8: Model statistics overview for edge rounding height (FAWJ)

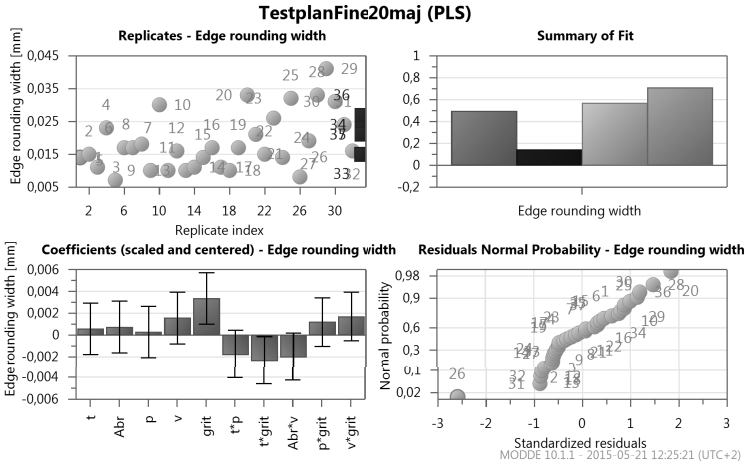

Figure F.9: Model statistics overview for edge rounding width (FAWJ)

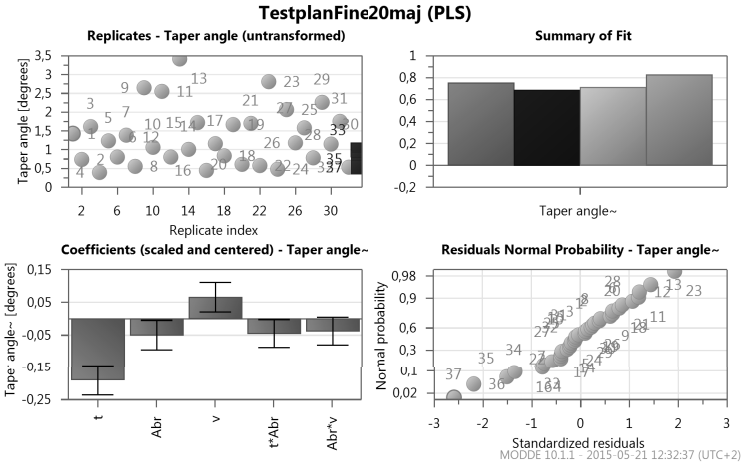

Figure F.10: Model statistics overview for taper angle (FAWJ)

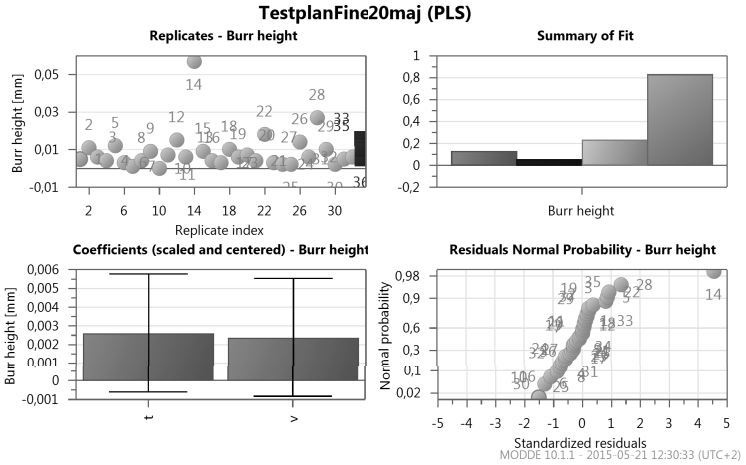

Figure F.11: Model statistics overview for burr length (FAWJ)

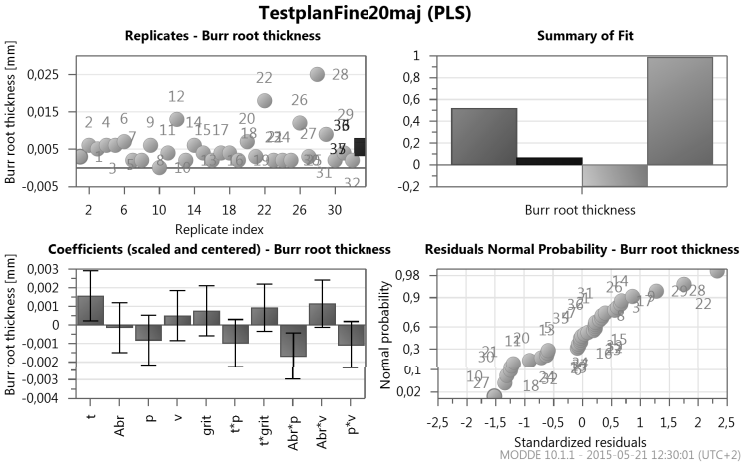

Figure F.12: Model statistics overview for burr root thickness (FAWJ)

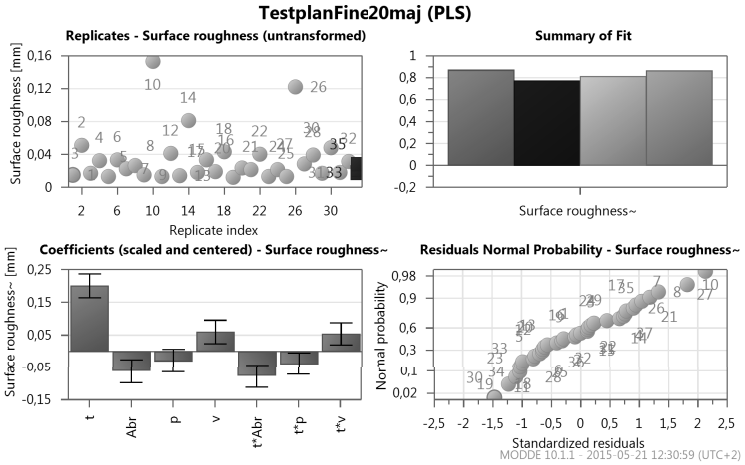

Figure F.13: Model statistics overview for surface roughness (FAWJ)

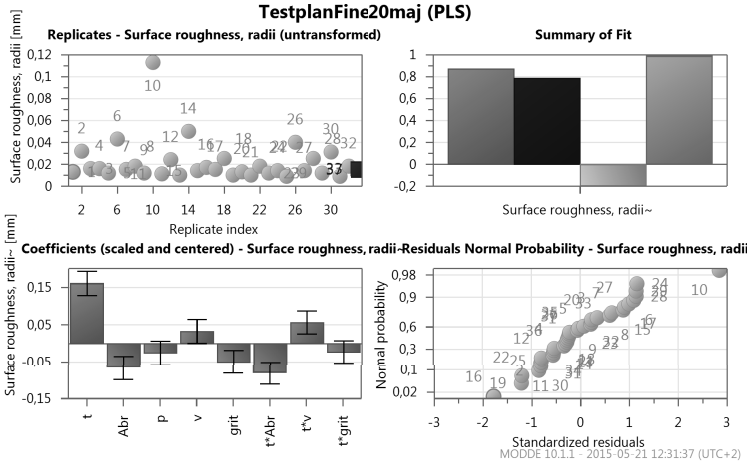

Figure F.14: Model statistics overview for surface roughness in radii (FAWJ)

G

Chemical Composition Mappings

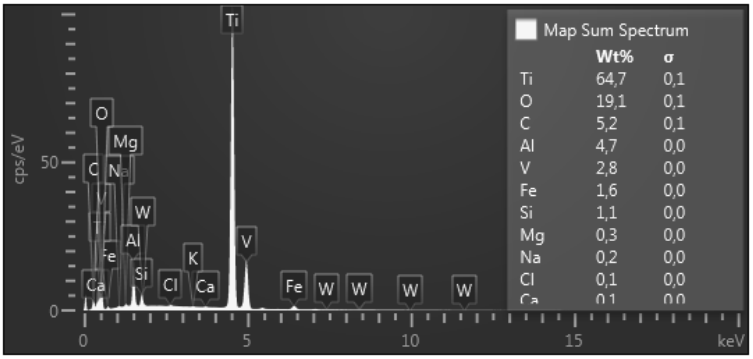

Figure G.1: Chemical composition mapping result for sample S1

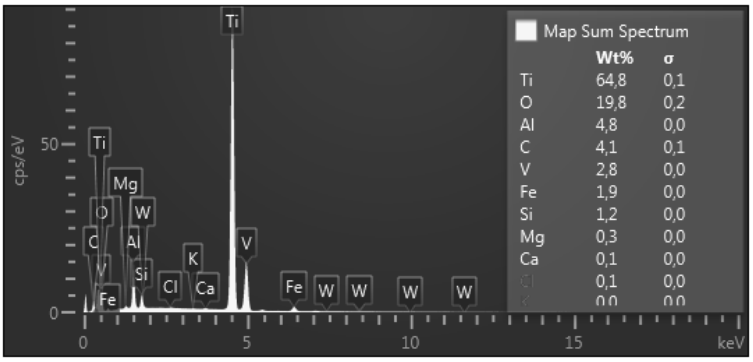

Figure G.2: Chemical composition mapping result for sample S2

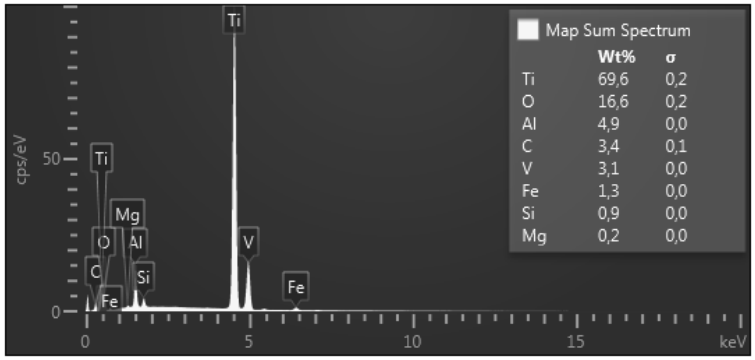

Figure G.3: Chemical composition mapping result for sample S15

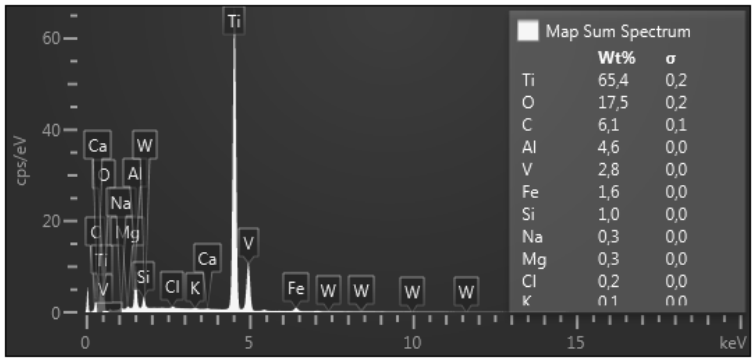

Figure G.4: Chemical composition mapping result for sample S16

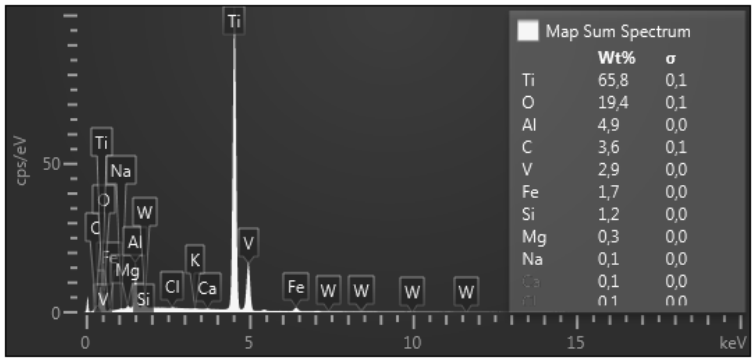

Figure G.5: Chemical composition mapping result for sample S17

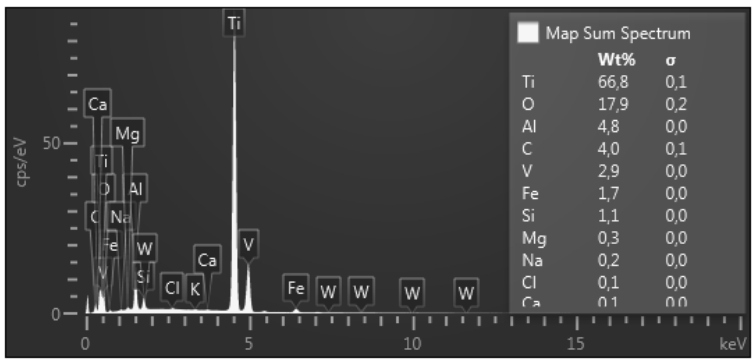

Figure G.6: Chemical composition mapping result for sample S18

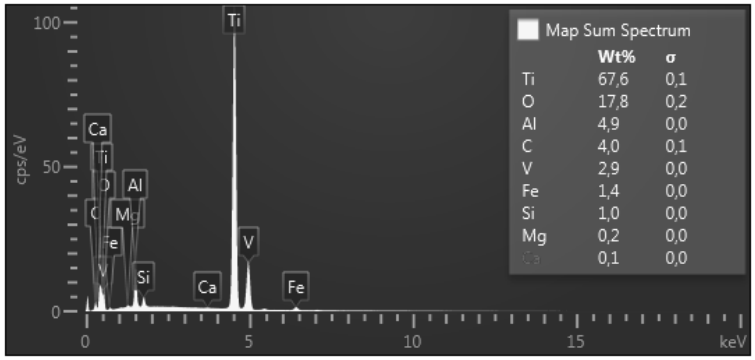

Figure G.7: Chemical composition mapping result for sample S31

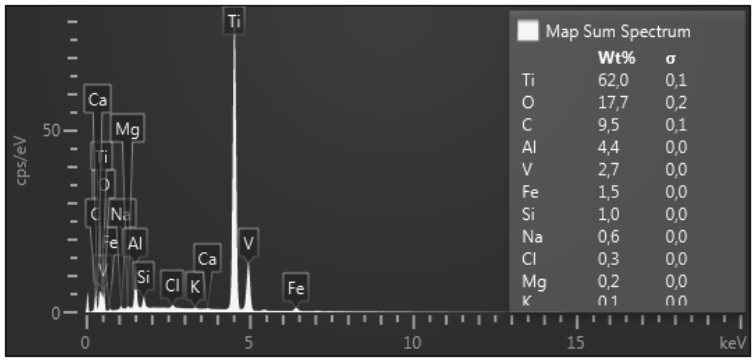

Figure G.8: Chemical composition mapping result for sample S32

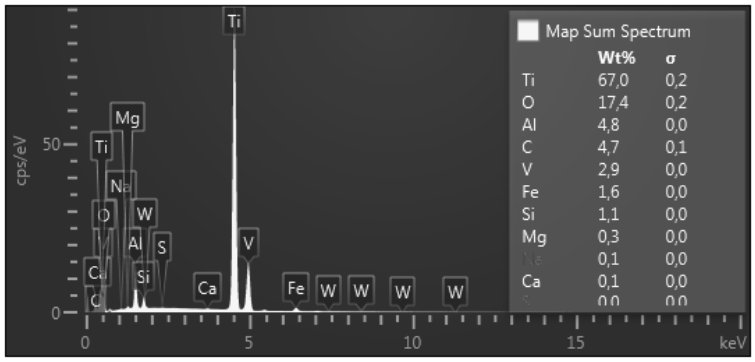

Figure G.9: Chemical composition mapping result for cleaned sample S32

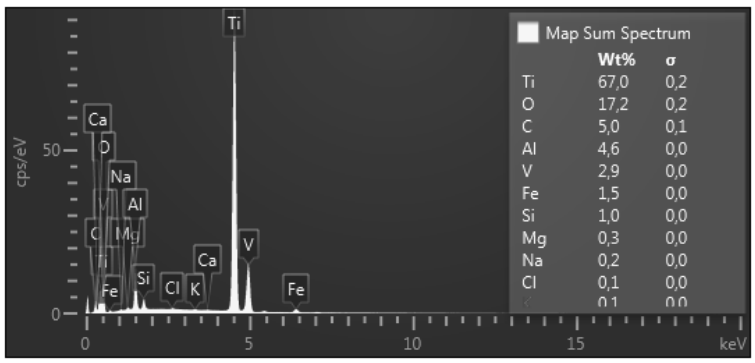

Figure G.10: Chemical composition mapping result for sample S33

H

Composition Mapping References

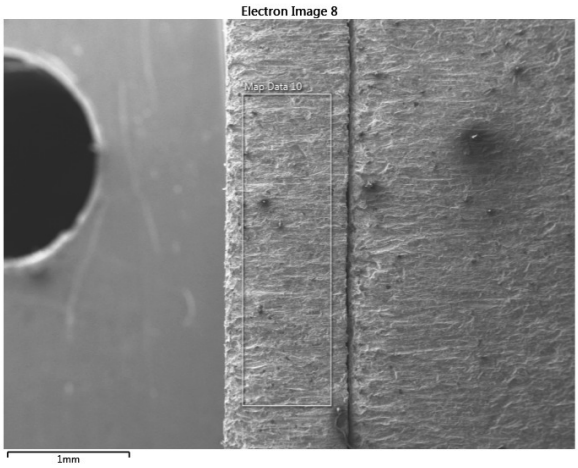

Figure H.1: Composition mapping reference picture for sample S1

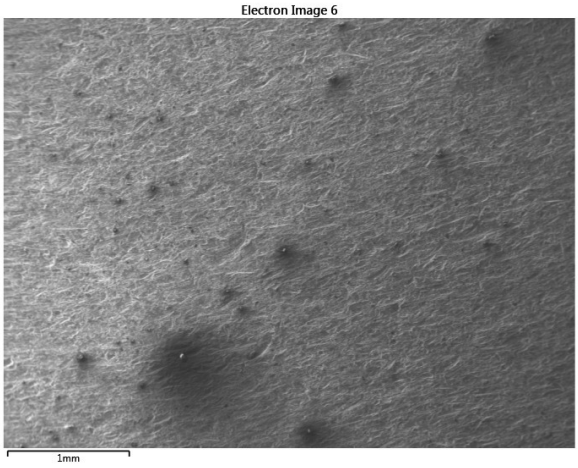

Figure H.2: Composition mapping reference picture for sample S2

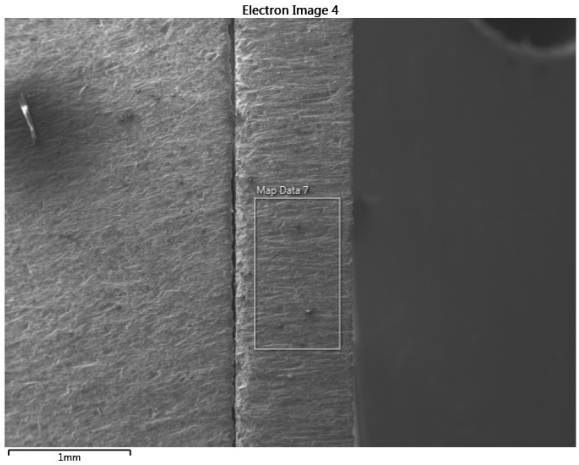

Figure H.3: Composition mapping reference picture for sample S15

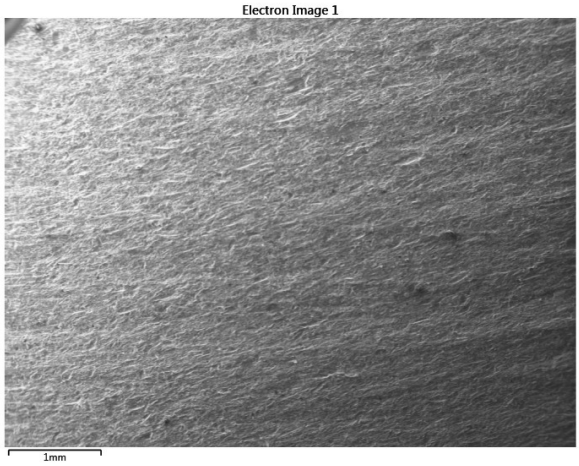

Figure H.4: Composition mapping reference picture for sample S16

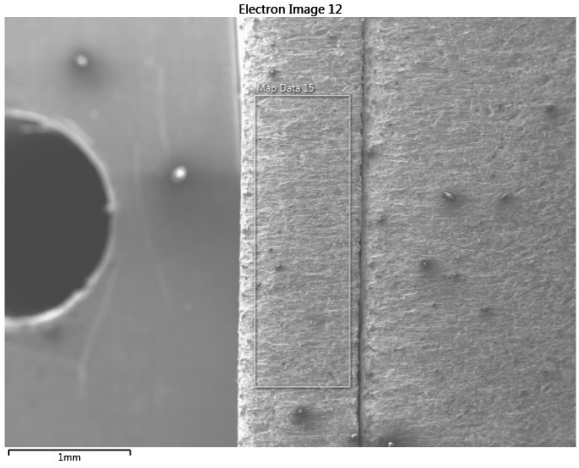

Figure H.5: Composition mapping reference picture for sample S17

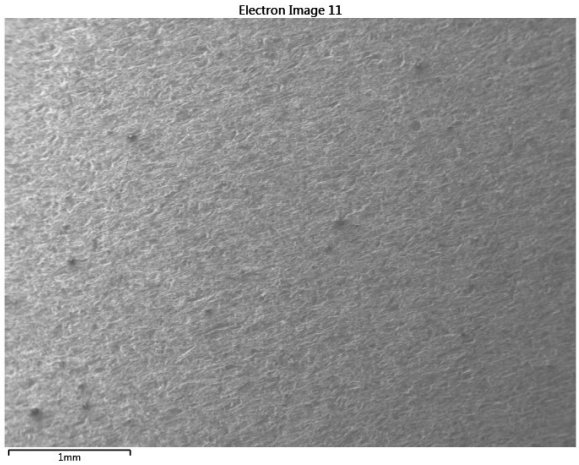

Figure H.6: Composition mapping reference picture for sample S18

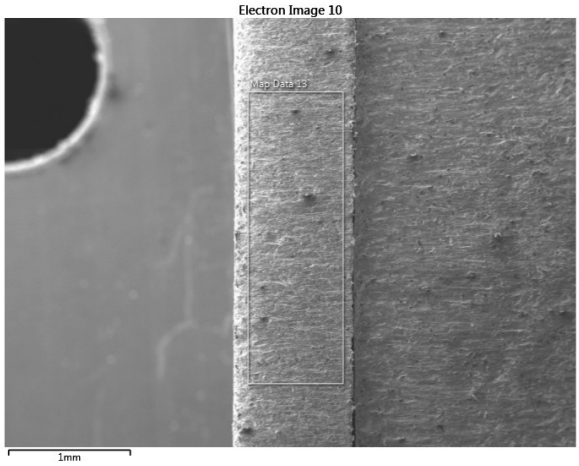

Figure H.7: Composition mapping reference picture for sample S31

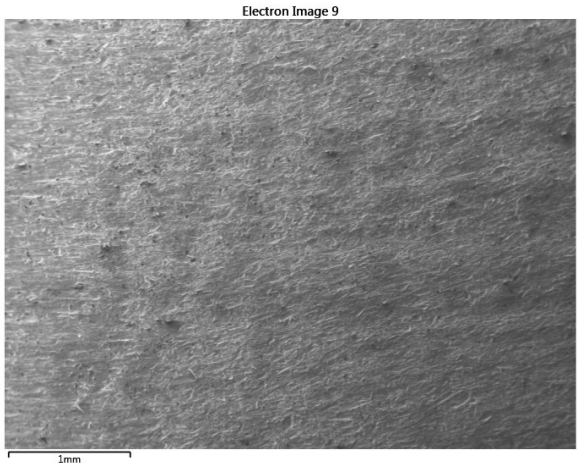

Figure H.8: Composition mapping reference picture for sample S32

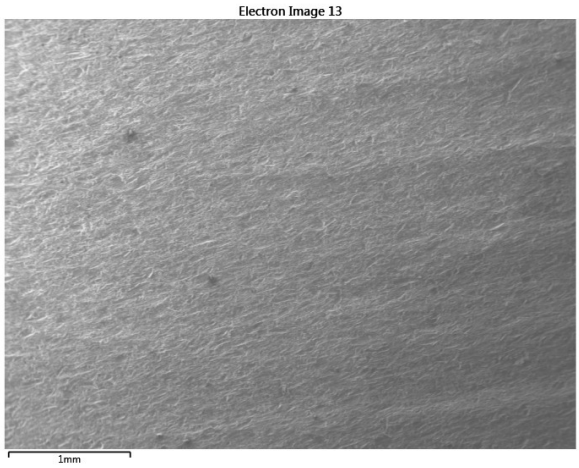

Figure H.9: Composition mapping reference picture for cleaned sample S32

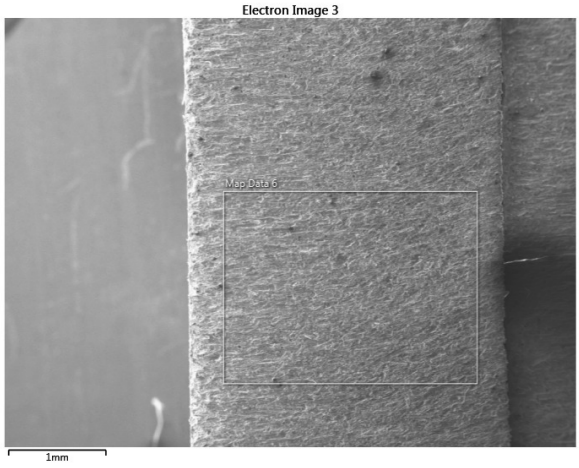

Figure H.10: Composition mapping reference picture for sample S33

I

Chemical Composition Point Scans

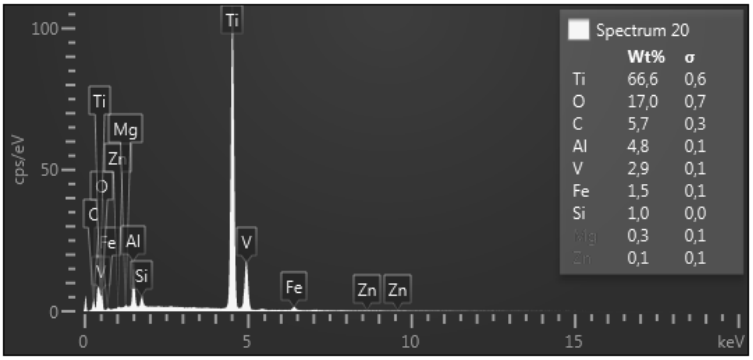

Figure I.1: Chemical composition point scan 1 result for sample S1

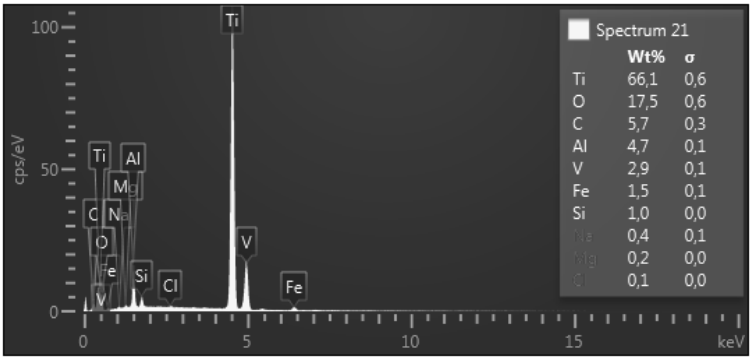

Figure I.2: Chemical composition point scan 2 result for sample S1

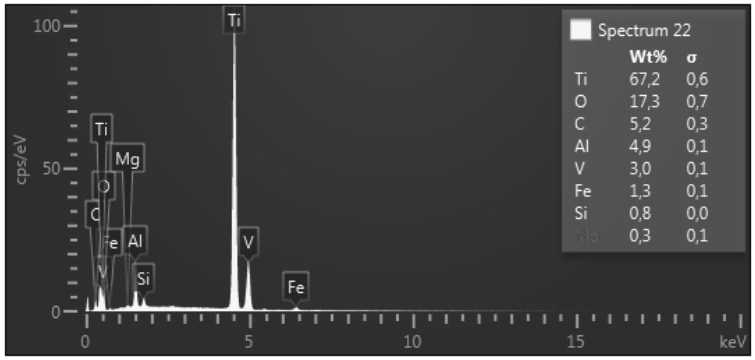

Figure I.3: Chemical composition point scan 3 result for sample S1

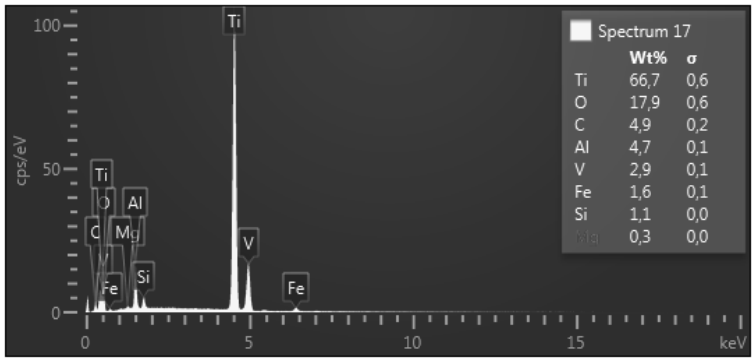

Figure I.4: Chemical composition point scan 1 result for sample S2

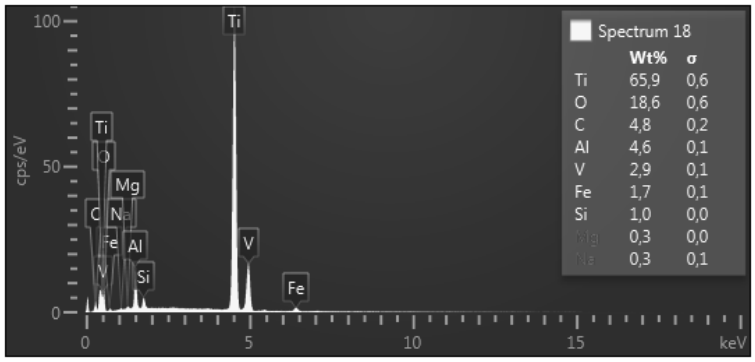

Figure I.5: Chemical composition point scan 2 result for sample S2

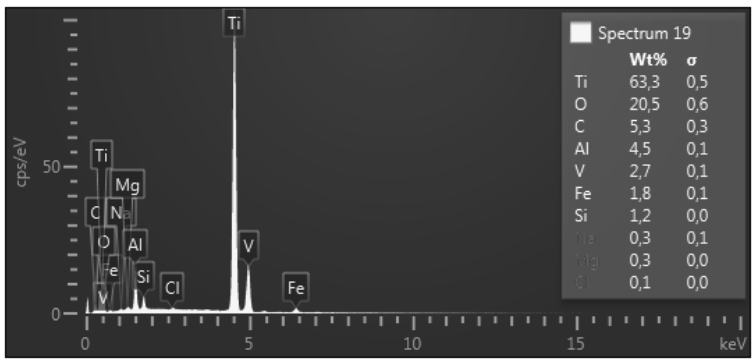

Figure I.6: Chemical composition point scan 3 result for sample S2

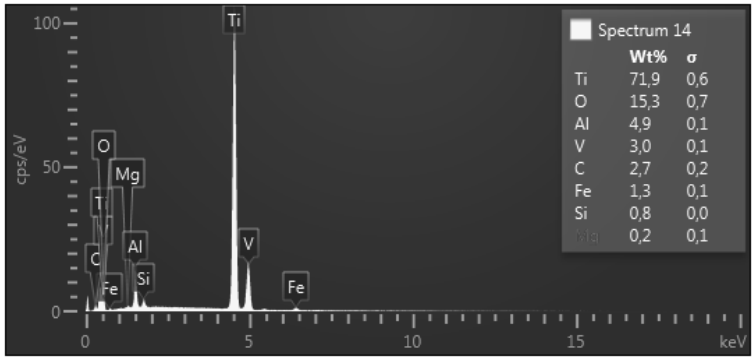

Figure I.7: Chemical composition point scan 1 result for sample S15

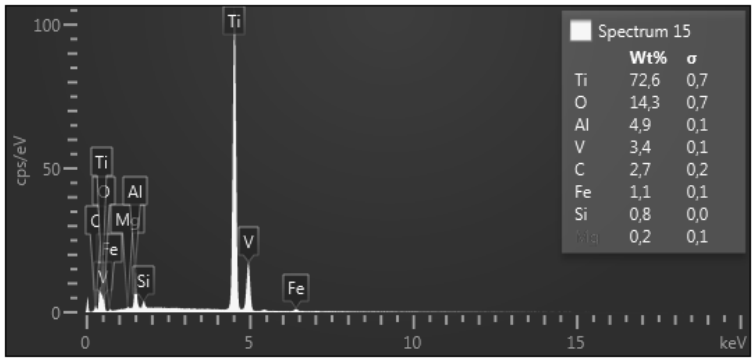

Figure I.8: Chemical composition point scan 2 result for sample S15

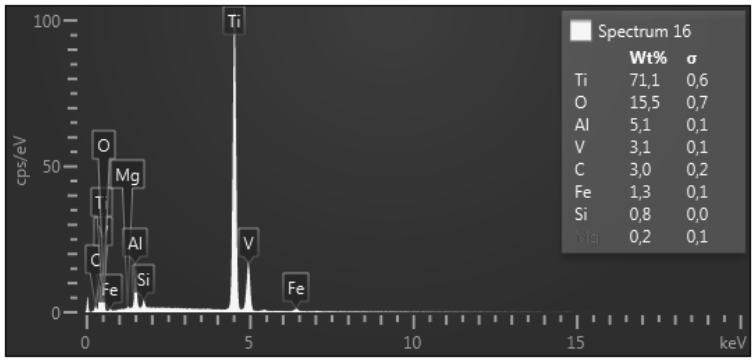

Figure I.9: Chemical composition point scan 3 result for sample S15

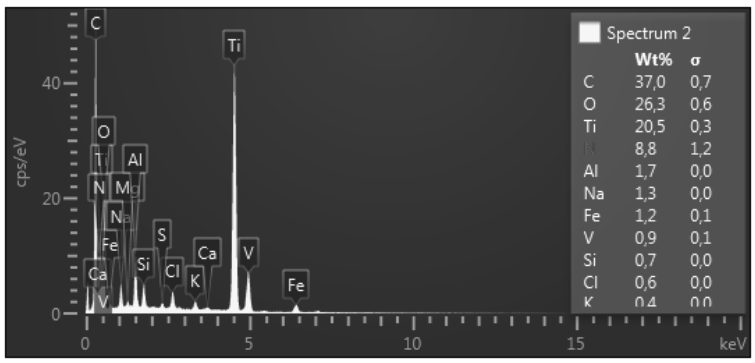

Figure I.10: Chemical composition point scan 1 result for sample S16

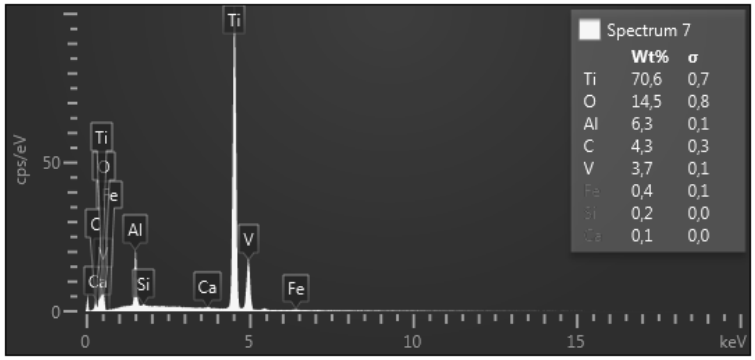

Figure I.11: Chemical composition point scan 2 result for sample S16

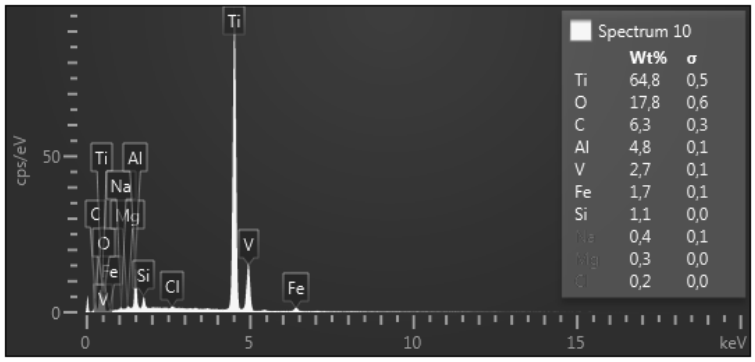

Figure I.12: Chemical composition point scan 3 result for sample S16

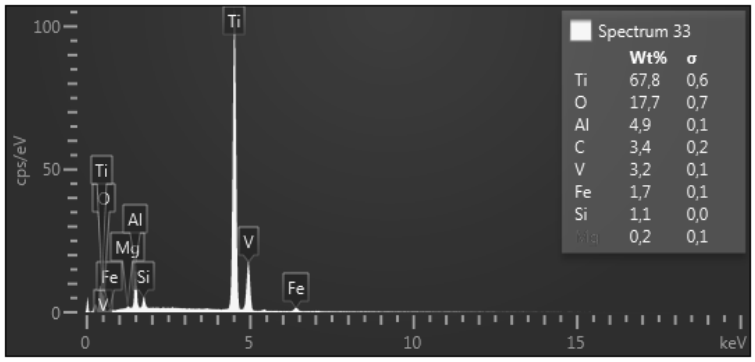

Figure I.13: Chemical composition point scan 1 result for sample S17

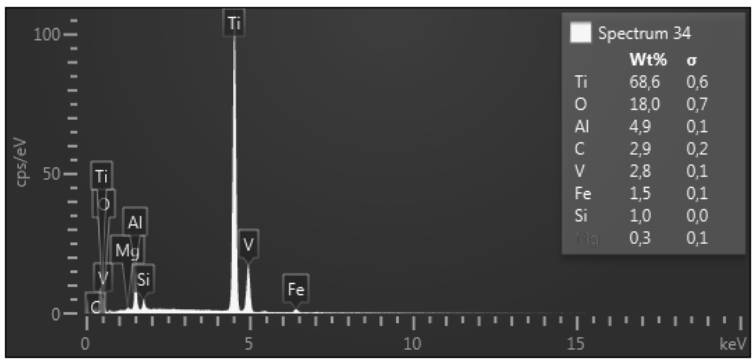

Figure I.14: Chemical composition point scan 2 result for sample S17

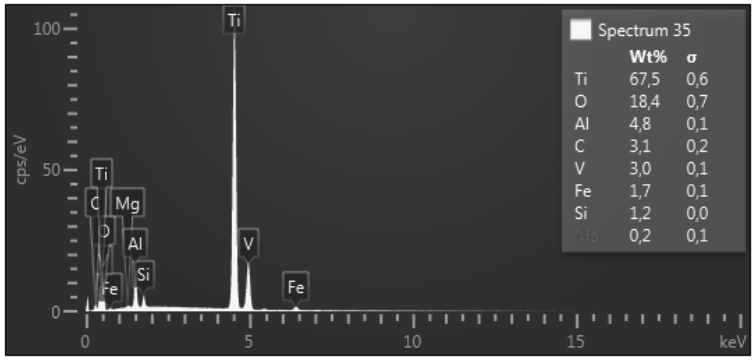

Figure I.15: Chemical composition point scan 3 result for sample S17

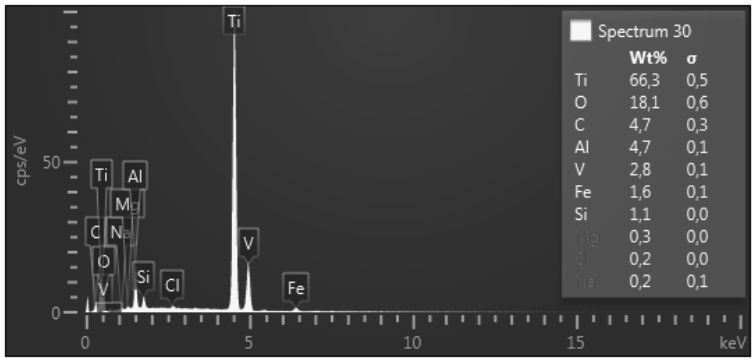

Figure I.16: Chemical composition point scan 1 result for sample S18

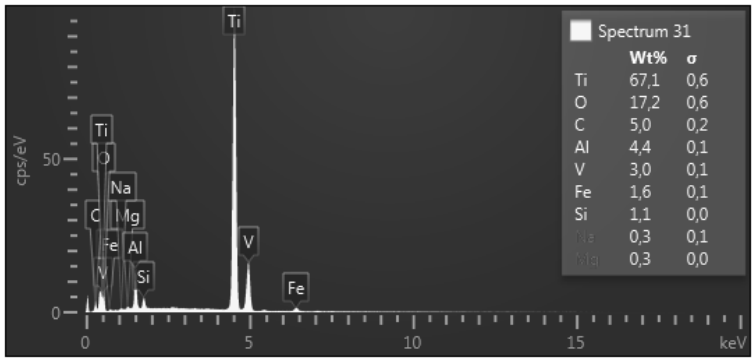

Figure I.17: Chemical composition point scan 2 result for sample S18

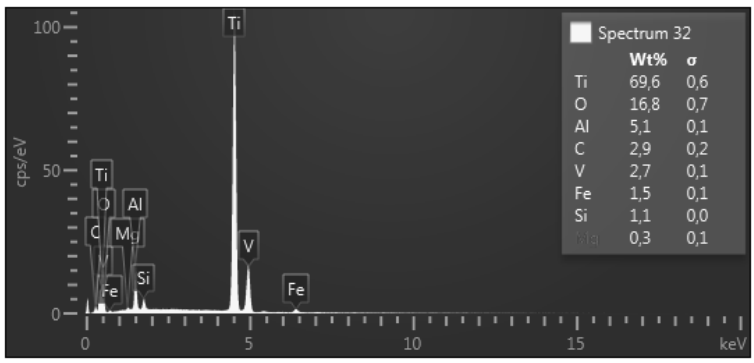

Figure I.18: Chemical composition point scan 3 result for sample S18

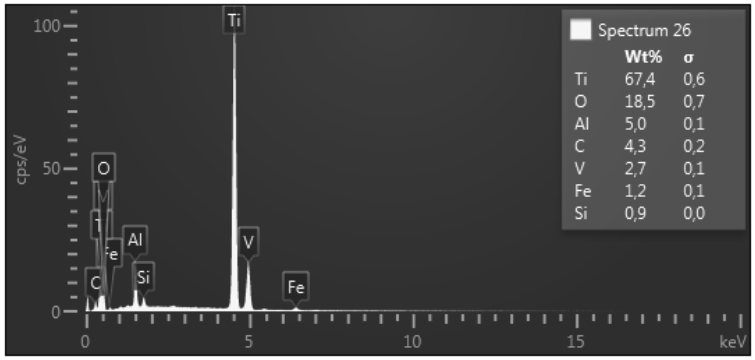

Figure I.19: Chemical composition point scan 1 result for sample S31

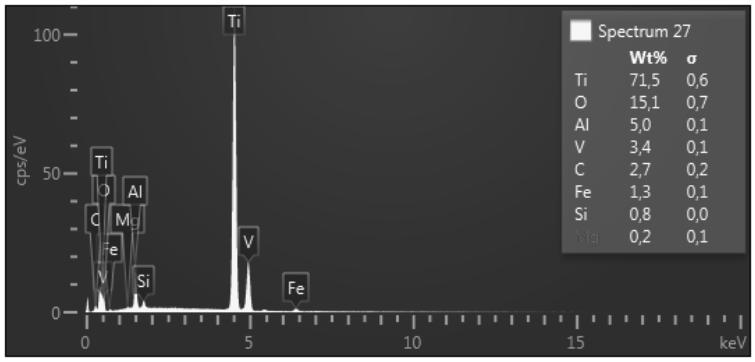

Figure I.20: Chemical composition point scan 2 result for sample S31

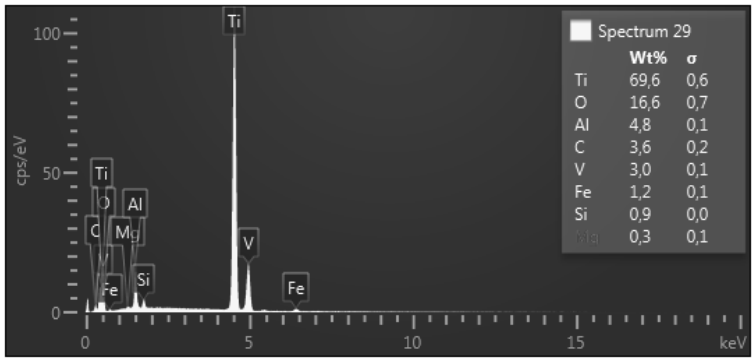

Figure I.21: Chemical composition point scan 3 result for sample S31

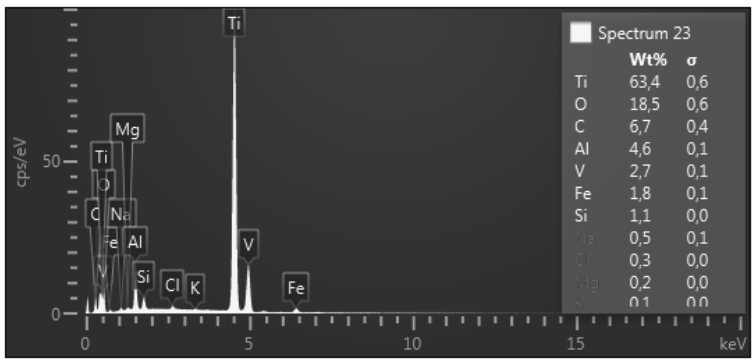

Figure I.22: Chemical composition point scan 1 result for sample S32

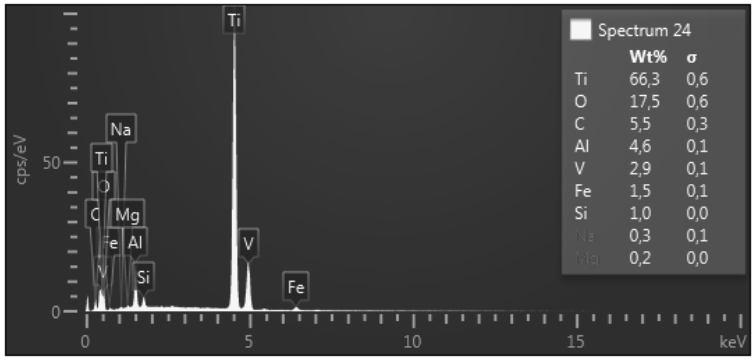

Figure I.23: Chemical composition point scan 2 result for sample S32

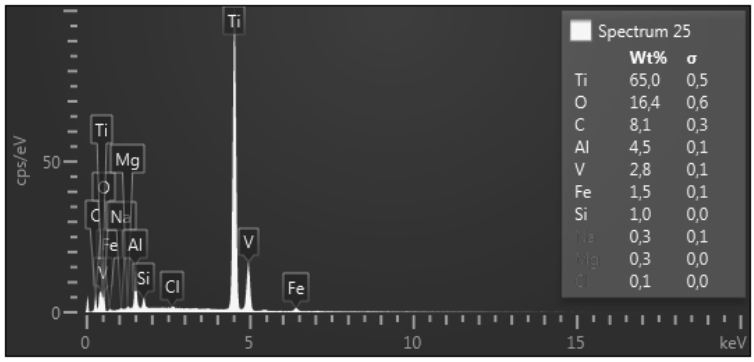

Figure I.24: Chemical composition point scan 3 result for sample S32

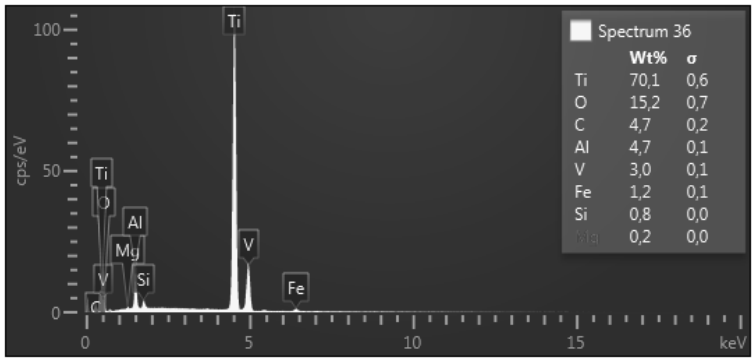

Figure I.25: Chemical composition point scan 1 result for cleaned sample S32

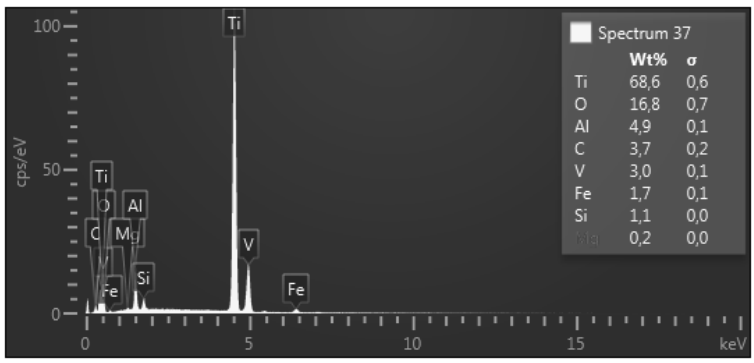

Figure I.26: Chemical composition point scan 2 result for cleaned sample S32

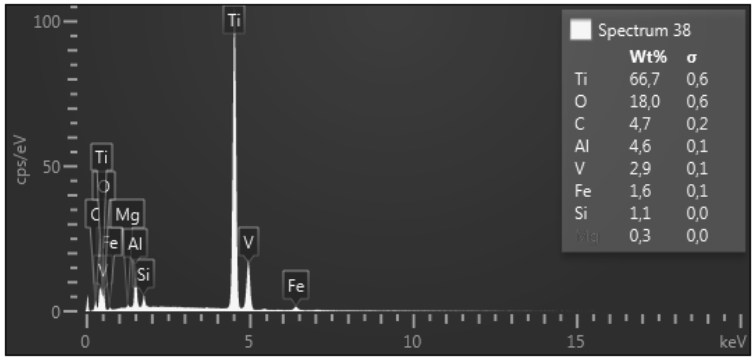

Figure I.27: Chemical composition point scan 3 result for cleaned sample S32

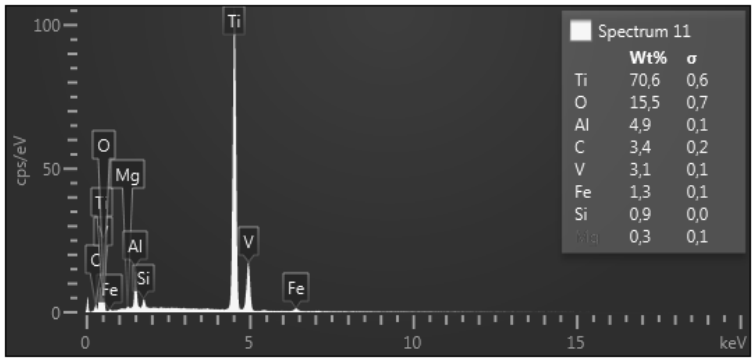

Figure I.28: Chemical composition point scan 1 result for sample S33

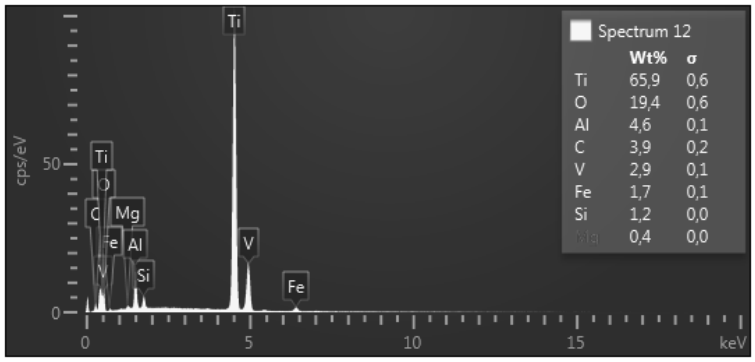

Figure I.29: Chemical composition point scan 2 result for sample S33

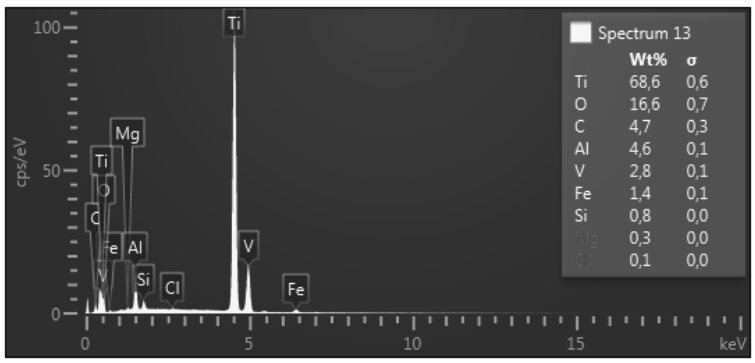

Figure I.30: Chemical composition point scan 3 result for sample S33

J

Abrasive Feed Calibration

The data in this chapter have been excluded from this version of the report, due to the secrecy of company property. The table below features the data used for calibration of feed rate in FAWJ experiments.

Table J.1: Abrasive feed calibration result sheet

Grit size [mesh]	Measure time [min]	Input feed [g/min]	Bag weight [g]	Measured weight [g]	Resulting weight [g]	Resulting feed [g/min]
150	-	-	-	-	-	-
150	-	-	-	-	-	-
150	-	-	-	-	-	-
200	-	-	-	-	-	-
200	-	-	-	-	-	-
200	-	-	-	-	-	-
230	-	-	-	-	-	-
230	-	-	-	-	-	-
230	-	-	-	-	-	-